UNIVERSITÀ DEGLI STUDI DI PAVIA

FACULTY OF ENGINEERING

Department of Electrical, Computer and Biomedical Engineering

PhD thesis in Microelectronics

Highly Linear Filtering TIA for 5G wireless standard and beyond

Advisors:
Prof. Rinaldo Castello
Prof. Danilo Manstretta

PhD thesis of
Nimesh Nadishka Miral

Academic Year 2021/2022

Declaration of Authorship

I, , declare that this thesis titled, and the work presented in it are my own. I confirm that:

- This work was done wholly or mainly while in candidature for a research degree at this University.
- Where any part of this thesis has previously been submitted for a degree or any other qualification at this University or any other institution, this has been clearly stated.
- Where I have consulted the published work of others, this is always clearly attributed.
- Where I have quoted from the work of others, the source is always given. With the exception of such quotations, this thesis is entirely my own work.
- I have acknowledged all main sources of help.
- Where the thesis is based on work done by myself jointly with others, I have made clear exactly what was done by others and what I have contributed myself.

Signed:

Date:

UNIVERSITÀ DEGLI STUDI DI PAVIA

Abstract

Facoltà di Ingegneria

Dipartimento di Ingegneria Industriale e dell'Informazione

Design of

by Nimesh Nadishka Miral

The demand for high data rates in emerging wireless standards is a result of the growing number of wireless device subscribers. This demand is met by increasing the channel bandwidth in accordance with historical trends. As MIMO technology advances, more bands and antennas are expected to be used. The most recent 5G standard makes use of mm-wave bands above 24GHz to expand the channel bandwidth. Channel bandwidth can exceed 2GHz when carrier aggregation is used. From the receiver's point of view, this makes the baseband filter's design, which is often a TIA, more difficult. This is due to the fact that as the bandwidth approaches the GHz range, the TIA's UGBW should be more than 5GHz and it should have a high loop gain up to high frequencies. A closed-loop TIA with configurable bandwidth up to 1.5GHz is described in this scenario. Operational Transconductance Amplifier (OTA) closed in shunt-feedback is the foundation of the TIA. The proposed OTA is based on FeedForward topology (FF) together with inductive peaking technique to ensure stability rather than using the traditional Miller compensation technique. The TIA is able to produce GLoop unity gain bandwidth of 7.5GHz and high loop gain (i.e. 27dB @ 1GHz) using this method. The mixer and LNA's linearity will benefit from this. Utilizing TSMC 28nm CMOS technology, a prototype has been created using this methodology. The output integrated noise from 20MHz to 1.5GHz is lower than $300\mu V_{rms}$ with a power consumption of 17mW, and the TIA achieves In-band OIP3 of 33dBm.
Additionally, a direct-conversion receiver for 5G applications is described. The 7GHz RF signal is down-converted to baseband by the receiver. Two cascaded LNTAs based on a common-gate transformer-based design make up the front-end. With an RF gain of 80mS and a gain variability of 31dB, it provides wideband matching from 6GHz to 8GHz. A double-balanced passive mixer is driven by the LNTA. The channel bandwidth from 50MHz to 2GHz is covered

by two baseband paths. The first path, called as the low frequency path (LF), covers the channel bandwidth ranging from 50MHz to 400 MHz. In contrast, the second path, called as the high frequency path (HF), covers the channel bandwidth between 800MHz and 2GHz. Two baseband provide gain variability of 14dB, making the overall receiver able to have a gain configurability from 45dB to 0dB. Out-of-band (OOB) selectivity at 4 times the band-edge is greater than 33dB for each configurability. When the gain is at its maximum, the noise figure is less than 5.8dB, and the slope of the noise rise as the gain falls is less than 0.7dB/dB. The receiver guarantee an IB-OIP3 larger than 21dBm for any gain configuration. The receiver has been implemented in TSMC 28nm CMOS technology, consuming 51mW for LF path and 68mW for HF path. The measurement results are in perfect accordance with the requirements of the design.

Contents

List of Figures

Introduction

Mobile communication systems are now widely used in people's daily lives. The tremendous increase in wireless system subscriptions has pushed the broad adoption of mobile devices over time and drastically increased the amount of data that networks must process. Even the services offered have expanded, moving beyond the most basic technologies like phone conversations to the most advanced ones like augmented reality and the Internet of Things (IoT). This is made feasible by the increasing data rate brought on by the development of mobile standards, starting with GSM and ultimately with 5G. Modern standards are improved in order to accomplish this by increasing the channel bandwidth, utilizing multiple operating bands, or using different antennas on the same device to send and receive data (MIMO). The 5G standard uses mm-wave to provide channel bandwidth of 2GHz with carrier aggregation in order to enhance the bandwidth. These enhancements make transceiver design more challenging and impose very strict requirements on them, particularly on the receivers. As a result of using multiple bands, the receiver must be able to handle strong out-of-band (OOB) signals without compromising the desired signal. With many antennas, there is a possibility that the transmitted signal will be coupled with the receiving antennas, causing a significant interference in the receiver's input that could de-sensitize it. RF filters were employed in the classic receiver chain to reduce the unwanted OOB signals. Due to their size, these filters raise system complexity and chip cost. Due of these factors, creating a single wide-band receiver that can operate over many bands has become increasingly desirable in recent years. This necessitates paying close attention to the receivers' design since they must be able to handle strong, unfiltered OOB signals. The baseband portion needs special consideration since it must filter the unfiltered OOB signal without clipping or slewing while maintaining high linearity, which is more challenging as the channel bandwidth increases. The design of the Trans-Impedance Amplifier (TIA), which handles channel select filtering in the baseband region, is covered in this study. Operational Transconductance Amplifier (OTA) with parallel R-C feedback is the foun-

dation of the TIA architecture. Inductive peaking is used in the design along with the FeedForward (FF) topology to provide stability. This method enables the TIA to function over a wide bandwidth (upto 1.5GHz) while maintaining high loop gain up to high frequencies, which guarantees good linearity (33dBm IB-OIP3).
A wide-band direct-conversion receiver design for 5G applications is also presented. The 7GHz RF signal is downconverted to baseband by the receiver. The receiver can provide more than 33dB of OOB selectivity at frequencies four times the band-edge, covering an RF bandwidth of 50MHz to 2GHz. The following summarizes how this thesis is structured:

Chapter 1 outlines the key requirements and metrics that must be taken into account while designing a wireless receiver. The development of the wireless system is then described in great detail. This chapter presents the progression toward broad channel bandwidth and the specifications included in the most recent wireless standard (5G), with an emphasis on the receiver specifications.

Chapter 2 for 5G and future generations, a closed-loop 1.5GHz bandwidth TIA is described in detail. Particular attention is devoted in the design of the OTA topology and the technique used to ensure the stability. Following the design presentation, the measurements of the prototype built using 28nm CMOS technology are given. The linearity and noise performance of this TIA are provided.

Chpater 3 the 5G wireless receiver design is described. Two cascaded LNTA with a cross-coupled CG architecture make up the front-end. The first LNTA is built around a trifiliar transformer, which provides matching and bias of the LNTA. The second LNTA, which was preceded by a transformer that provide current gain, so that reduces power consumption and enhances noise performance is described. The design of two baseband sections that cover the RF bandwidth range of 50MHz to 2GHz is discussed in the last section. The first path, which includes first order TIA after the Racuh filter, covers channel bandwidth from 50 MHz to 400 MHz. The second path, on the other hand, uses a 2nd-order open loop filter followed by a 1st order TIA to cover channel bandwidth from 800MHz to 2GHz.

Chapter 4 presents the measurement results for the receiver discussed in Chapter 4. TSMC 28nm CMOS technology was used to implement the receiver.

The receiver measurement setup will be explained first, and the measurement results for both the high frequency (HF) and low frequency (LF) baseband paths will then be given. The measured receiver performance in comparison to the initial specifications will then be shown.

Chapter 1

Evolution and Design Requirements of Wireless Standards

Abstract
In order to accommodate an increasing number of users and offer more services, wireless communications have evolved over time. To increase the data rate, several additional features have been created, necessitating complex wireless transceiver architecture. The main metrics for receiver design are covered in this chapter. An overview of the development of wireless standards is given, with special attention paid to the specifications necessary for designing a receiver for user equipment.

1.1 Main Communication Metrics

The progress of the cellular system over the past decade has taken it from the First Generation to the Most Evolved Standard (5G) due to the growing number of subscribers in wireless communication systems. This progress requires a lot of operations that has to be performed both in analog and in digital domain. These could include data modulation and transmission on the transmitter (TX) side or signal detection and original data reconstruction on the receiver (RX) side. As number of wireless communication increases, the wireless environment becomes crowded, which resulted in strict requirements for each block in the receiver. Such requirements are provided in the standard and correspond to metrics that are unique to each block. To evaluate the wireless transceiver performances, certain fundamental design parameters are

discussed in the following subsections.

1.1.1 Sensitivity and Noise Figure

The receiver has to detect a small signal, but in the presence of significant noise, the signal cannot be detected with a quality that is acceptable. The parameter known as sensitivity specifies the minimum signal level that a receiver can detect while maintaining "acceptable quality" [1]. The signal-to-noise ratio that the system can tolerate determines the "acceptable quality". Sensitivity is defined as following:

$$P_{sens[dBm]} = P_{RS[dBm/Hz]} + NF_{[dB]} + 10logB + SNRmin_{[dB]}, \tag{1.1}$$

where $P_{RS[dBm/Hz]}$ is the noise power spectral density of the source (i.e. antenna), $SNR_{min[dB]}$ is the minimum required Signal to Noise ratio at the output, and B is the channel bandwidth expressed in Hz. NF is the noise figure of the receiver defined as the ratio of the SNR at the input and at the output.

$$NF_{[dB]} = 10log\left(\frac{SNR_{in}}{SNR_{out}}\right). \tag{1.2}$$

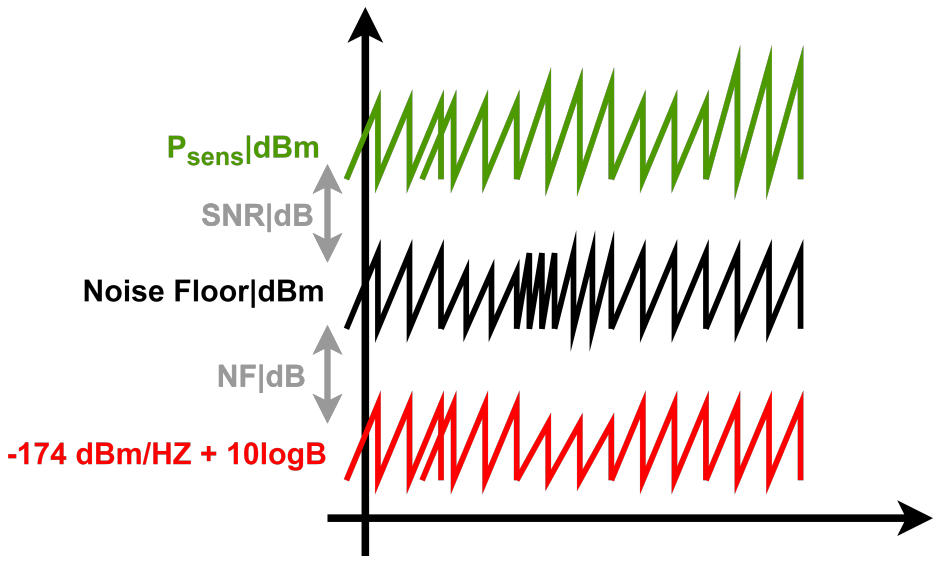

Figure 1.1: An illustration of the relationship between sensitivity, SNR, noise floor, and NF in the scenario that the receiver and antenna are matched.

The system noise floor is represented by the first three terms in equation 1.1. If the receiver is matched to the antenna, P_{RS} corresponds to KT, which equals $-174dBm/Hz$. Therefore, the noise floor becomes:

$$P_{sens[dBm]} = -174dBm/Hz + NF_{[dB]} + 10logB. \tag{1.3}$$

Figure 1.1 shows this concept. The bit-error rate specified in the standard is what determines the minimum needed SNR, which is dependent on the employed modulation scheme. Since the detection becomes more sensitive to noise as the constellation points get closer, higher SNR is required. The maximum tolerable NF, which is the real requirement for the RF designer, can be calculated using the equation 1.1 after the minimum SNR and sensitivity are known.

1.1.2 Non-Linearity

Non-linearity is another significant effect to take into account while designing the receiver. Although linear approximations could usually be used to model analog and RF circuits for small signal operations, nonlinearities typically result in interesting and important phenomena that cannot be predicted by

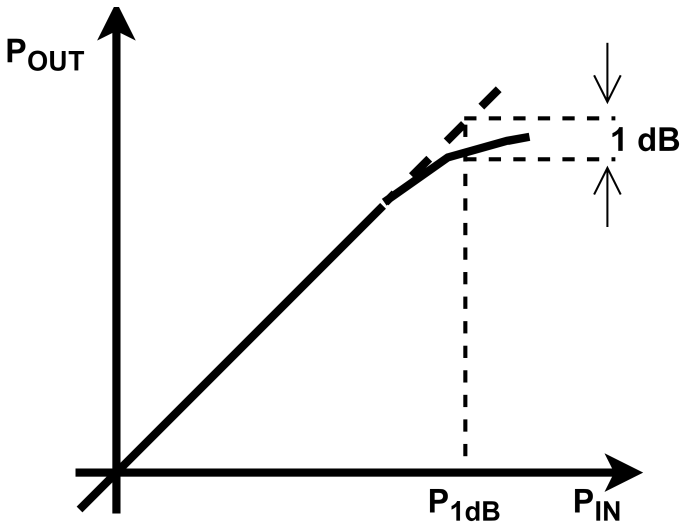

Figure 1.2: The IP3 (third-order intercept point) is defined as the intersection of the extended output power curves of the Fundamental and IM3 products on a log-scale.

small-signal models. The input/output characteristic of analog or RF circuit can be approximated with a Taylor's series expansion:

$$y(t) \approx \alpha_1 x(t) + \alpha_2 x^2(t) + \alpha_3 x^3(t). \tag{1.4}$$

where $x(t)$ is the input signal, $y(t)$ is the output signal, α_2 and α_3 are the second and third non-linear coefficient and α_1 is the small signal gain of the circuit when a small signal is applied. According to the equation 1.4, when a sinusoidal signal with frequency ω_0 is applied to the input of the circuit, a product of sinusoidal signals at integer multiple of ω_0 (harmonics) appears to the output. Substituting $x(t)$ with $A\,cos(\omega_0 t)$ in 1.4, $y(t)$ results in:

$$y(t) = \alpha_2 \frac{A^2}{2} + \left(\alpha_1 + \frac{3}{4}\alpha_3 A^2\right) A cos(\omega_0 t) + \frac{1}{2}\alpha_2 A^2 cos(2\omega_0 t) + \frac{3}{4}\alpha_3 A^3 cos(3\omega_0 t). \tag{1.5}$$

In the equation 1.5, the first component on the right side is a dc quantity resulting from second-order non-linearity, the second term is referred to as the fundamental, and the third and fourth terms are the second and third order harmonics. It is clear from equation(1.5) that the gain of the fundamental depends not only on α_1, but also on α_3, which changes dramatically as amplitude (A) increases. Since α_1 and α_3 have the opposite sign in the fully differential situation, which is typically the case, the gain decreases as the amplitude increases. As a result, the input/output characteristic, as represented in figure 1.2, bends as the input amplitude increases. Therefore, the term associated with the third order distortion compress the gain. This effect is evaluated using a metric known as the 1-dB compression point, which is defined as the input amplitude level at which the gain decreases by 1 dB. The input 1-dB compression point is computed by taking the gain at the fundamental component $\left(\alpha_1 + \frac{3}{4}\alpha_3 A_{IN,1dB}^2\right)$ and equate it to 1dB, resulting in $A_{IN,1dB} = \sqrt{0.145|\frac{\alpha_1}{\alpha_3}|}$.

Strong undesired signal (interferer) present along with desired signal is another consequence that results in gain compression. To explain this effect, $x(t) = A_0 cos(\omega_0 t) + A_1 cos(\omega_1 t)$ is substituted in the equation 1.4, and the term corresponding to the fundamental tone becomes:

$$y(t) = \left(\alpha_1 + \frac{3}{4}\alpha_3 A_0^2 + \frac{3}{2}\alpha_3 A_1^2\right) A_0\, cos(\omega_0 t) + ... \tag{1.6}$$

This equation (1.6) makes it apparent that the gain of the desired signal decreases as the amplitude of the interference increases. Desensitization is the

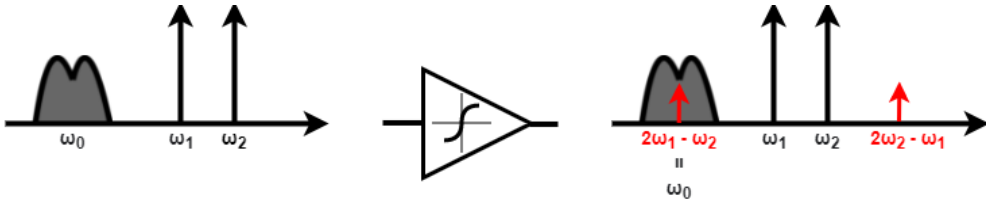

Figure 1.3: The Description of IM3 falling onto desired band.

term of this effect, which reduce the SNR of the receiver.

An other consequence of non-linearity is the third-order intermodulation (IM3). This occurs when the desired signal is present along with two tones at angular frequency ω_1 and ω_2. If $x(t) = A_1 cos\,(\omega_1 t) + A_2 cos\,(\omega_2 t)$ is subsitutude in 1.4, then $y(t)$ becomes:

$$\begin{aligned} y(t) = &\alpha_1 \left(A_1 cos\omega_1 t \,+\, A_2 cos\omega_2 t\right) + \alpha_2 \left(A_1 cos\omega_1 t \,+\, A_2 cos\omega_2 t\right)^2 + \\ &+\, \alpha_3 \left(A_1 cos\omega_1 t \,+\, A_2 cos\omega_2 t\right)^3, \end{aligned} \tag{1.7}$$

which has components (associated with third order non-linearity) at $2\omega_1 - \omega_2$ and $2\omega_2 - \omega_1$:

$$\begin{aligned} y(t) \,=\, \cdots + \frac{3}{4}\alpha_3\, A_1^2 A_2\, cos\,(2\omega_1 t + \omega_2 t) \,+\, \frac{3}{4}\alpha_3\, A_1^2 A_2\, cos\,(2\omega_1 t - \omega_2 t) \,+ \\ +\, \frac{3}{4}\alpha_3\, A_1 A_2^2\, cos\,(2\omega_2 t + \omega_1 t) \,+\, \frac{3}{4}\alpha_3\, A_1 A_2^2\, cos\,(2\omega_2 t - \omega_1 t) \,+\, \cdots \end{aligned} \tag{1.8}$$

This mechanism is shown graphically in figure 1.3, where it is shown that the IM3 product may fall onto the desired band if $\omega_0 = 2\omega_1 - \omega_2$, which would reduce SNR. Receiver IM3 performance is evaluated using a two-tone test, in which two sinusoids of equal amplitude (A) are applied to the receiver input and the receiver IM3 is measured. From 1.8, it is clear that IM3 increases as A^3, which means that the relative ratio between the Fundamental and IM3 grows as A^2. Therefore, the IM3 is expressed in terms of IIP3 because it is preferable to have a quantity that is independent of amplitude A. This number represents the input amplitude level at which the amplitude of the input referred fundamental tone and the amplitude of the IM3 are equals at the output. The input level at which this occurs is known as the "input third intercept point (IIP3)", as shown in figure 1.4. In reality, higher-order nonlinearities may appear as amplitude A increases, causing the slopes of both

the fundamental and IM3 functions to deviate from the expected value. As shown in figure 1.4, in order to measure IIP3, a low value of amplitude (A) is first applied to ensure that higher-order nonlinearities are negligible after this amplitude is increased. Then, the amplitudes of the fundamentals and IM3 products are plotted on a log-log scale, and these plots are extrapolated based on their slop (1 and 3). It must be noted that there should be a 3-dB increase in IM3 for every 1-dB increase in input amplitude in order to ensure that the signal keeps below higher-order nonlinearities. Using this method, IIP3 may be calculated as:

$$A_{IIP3[dBV]} = A_{[dBV]} + \frac{A_{[dBV]} - A_{IM3[dBV]}}{2}, \tag{1.9}$$

where $A_{IIP3[dBV]}$ is actual IIP3, $A_{[dBV]}$ and $A_{IM3[dBV]}$ corresponds to amplitude level of the fundamental and IM3 respectively, referred to the input of the receiver. The same formula can be used with the power level expressed in dBm.
Each wireless standard has a list of linearity tests that the receiver must fulfill. These indicate the amplitudes potential interferers as well as their distance from the desired signal band. From these specifications, linearity and compression requirements for the receiver can be constructed.

1.2 Evolution of Wireless Generation

In the recent decades, wireless networks have developed continuously to meet the needs of an ever-expanding users and an increasing demand for data services. Different technology and new concepts have been applied to accelerate this development. The primary drivers behind this evolution are increasing data rates and larger system capacities. The Shannon Theorem [2], which states that the bit rate is directly proportional to the channel bandwidth, provides the answer to the question of how these requirements are satisfied. Therefore, increasing bandwidth is the simplest way to increase data rate. New mobile generations have evolved using this approach by increasing the channel bandwidth and allocating multiple channels from the same or different band to single user, based on the notion of channel aggregation.
Using a higher order modulation approach, which results in more bits per symbol, is an alternative method of increasing data rate. Because of the noise, denser constellations make it more difficult to detect bits. The design becomes more difficult as a result of the increased SNR requirements.
The employment of many antennas on both the transmitter and receiver sides is actually one of the core technologies of the most recent wireless system

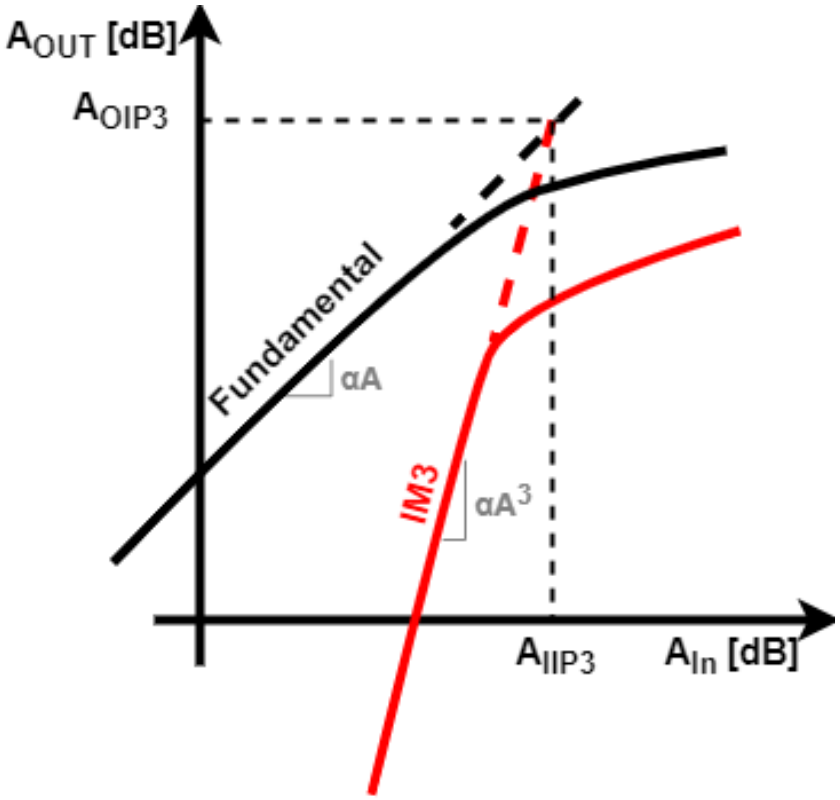

Figure 1.4: Definition IIP3 as the intersect between the Fundamental and IM3 on log-log scale .

(MIMO). This technique enables simultaneous transmission and reception of several data signals over a single radio channel. More transmitting and receiving antennas enhance the link quality, reliability, and throughput between the transmitter and the receiver. The radio link's robustness could be increased using this technique, which would also increase SNR.

1.2.1 Evolution from 1G to 3G

The mobile network's first generation (1G) was developed in 1980. It was developed to provide mobile services to mobile users and is based on analog transmission. 1G was composed of various standards, each based on a certain geographic region. For instance, Total Access Communication System (TACS) in western Europe, Nordic Mobile Telephone (NMT) in Scandinavian coun-

tries, and Advanced Mobile Phone (AMP) in North America. Similar characteristics were shared by these standards. As an example, the AMPS used FM modulation and operates in the $850\,MHz$ cellular band with 832 channels that are separated by $30\,kHz$ [3]. Frequency-Division-Duplexing (FDD), which uses two frequency bands for transmission and receiving, was employed by AMPS. The Frequency Division Multiple Access (FDMA) scheme, which assigns one channel per user and has poor capacity in crowded areas and requires huge frequency gaps to avoid interference, was used by 1G to address the multiple access problem. One channel is assigned to each user in the Frequency Division Multiple Access (FDMA) scheme, which was adopted by 1G to address the multiple access problem but has limited capacity in congested areas and requires wide frequency gaps to reduce interference. 1G cleared the way for the mass use of mobile phones despite other challenges that influence this network, such as poor hand-off reliability and safety issues [3] [4].

In 1990, the second generation (2G) was released. The primary improvement over 1G is that 2G is based on digital technology. This increased voice capacity and allowed for the adoption of new services including mobile fax, Short Messages Service (SMS), and voice mails. This standard is based on The Global System for Mobile Communication (GSM) [5], which was created as a unified wireless standard for Europe and has now become the most widely used cellular standard in the world. GSM uses FDD and works in a number of bands, including GSM900, GSM1800, and GSM1900. GSM uses GMSK modulation with a $270\,kbps$ data rate [6] and channels that are spaced $200\,kHz$ apart. GSM uses TDMA (Time Division Multiplexing Access), which is based on allocating the same channel in different time periods for different users, to increase the system capacity. These features enable the system capacity to be increased and the service to be extended to a large number of users.
GPRS (General Packet Radio Service), also known as 2.5G, is a development of GSM. In contrast to GSM, which relied on circuit switching, GPRS introduced packet switching. In this case, packet switching divides data to transmit into different blocks known as packets and these packets are transmitted across different paths to the receiver. This is in contrast to circuit switching, where a communication channel (circuit) is dedicated to two network nodes and it remains connected for the duration of the communication session. This limits the channel to the time required for packet transmission. MMS (Multimedia Messaging Service) and other internet-type services are made possible through GPRS. GSM was upgraded to EDGE (Enhanced Data Rates for GSM Evolution) in order to offer a higher data rate on a $200\,kHz$ channel. This de-

velopment is part of the 2.5G standard. The 8-PSK modulation scheme was used by EDGE to obtain a high data rate, which resulted in a data rate of 473 $kbit/s$ [7]. Because the points in the 8-PSK constellation are so close together, a higher SNR is needed to detect the received signal with a low BER (Bit Error Rate).

Code Division Multiple Access (CDMA) was used to establish the transition from second generation to third generation (3G). In CDMA, the signals can overlap in both time and frequency, in contrast to TDMA and FDMA. Each transmitter-receiver pair is given a special code at the beginning of every conversation. Before transmission, the data to be transmitted is multiplied by the assigned code, and the receiver uses the same code to decode the data. The total capacity of the system is better than TDMA and FDMA since multiple users can occupy the same bandwidth without interfering with one another, even though the code spreads the spectrum occupied by the transmitted signal (referred to as a "spread spectrum" approach). In the 3G standard, CDMA2000 and WCDMA (UMTS) were established as the two main standards. For example, the Universal Mobile Telecommunication System (UMTS) is characterized by 26 frequency bands that operate between 900 MHz and 2.1 GHz, with a 5 MHz channel spacing and the QPSK modulation scheme [8]. Data transmission at a rate of 2 Mbps was possible with UMTS. The demand for internet-type services, for which UMTS was designed, increased to the point that this standard needed to be updated. High-Speed Packet Access (HSPA) is the name of this standard, which offers a peak data rate of 14 Mbps [9].

1.2.2 4G LTE

With the introduction of Long Term Evolution (LTE) in 2008, the fourth generation of mobile networks (4G) was launched in order to increase capacity compared to UMTS and meet the growing demand for data services and internet access. Primary objectives of LTE were to increase data speeds, enhance bit rates at the cell edge, improve spectral efficiency, ensure greater spectrum flexibility, and lower mobile power consumption. LTE has evolved into LTE-Advanced (Release 10) and LTE-Advanced-Pro (Release 13 and 14). The ability to switch to alternative access technologies (like UMTS and GSM) is granted in order to ensure seamless coverage. In order to enable global use, LTE is defined over a broad range of frequency bands, from 700 MHz to 3.7 GHz. LTE provides larger channel bandwidth than earlier generations, continuing the patterns from the preceding generations. Variable carrier width, which has values ranging from 1.4 MHz to 20 MHz, in particular, offers more

flexibility. Consequently, this requires for a receiver with greater reconfigurability. LTE needs to solve multi-path transmission issues in order to reach higher data rates. In fact, due to inter-symbol-interference (ISI), signal quality decreases when the symbol time approaches the delay introduced by the channel. Orthogonal Frequency Division Multiplexing (OFDM) is a technique used by LTE to address this problem. This method involves first converting a high data rate stream from serial to N parallel streams with N times lower data rates. These are subsequently impressed on N different carrier frequencies, also known as sub-carriers. The total amount of spectrum occupation and data rate are the same as they were with single carrier modulation, but each of the N streams has a lower bit rate, making it possible to tolerate even more delay spread. In the first release of LTE (Rel. 8), only QPSK and 16QAM were used as modulation schemes. The most recent releases, however, combines these schemes with even higher-order modulation schemes, such as 64QAM and 256QAM.
Several significant LTE standard characteristics are discussed below:

1.2.2.1 MIMO

According to the Multiple-Input Multiple-Output (MIMO) technique, LTE uses multiple antennas in Base Station (BS) and User Equipment (UE) to further increase possible data rate. Utilizing MIMO has the following three benefits:

- **Spatial Multiplexing:** By sending the data payload in a separate stream across spatially separated antennas, the data rate is increased. At the receiving end, multiple streams are combined into a single data stream using additional spatially separated antennas. This increases efficiency and bit rate by allowing the transmission of many signal streams in parallell using the available frequency and time resources.

- **Spatial Diversity:** Utilizes different transmissions over multiple antennas to increase signal quality and mitigate the effects of multi-path fading.

- **Beam-forming:** The linear arrays that will allow the antenna to focus on a specific area are likely to be used in this MIMO mode, which is the most complicated one. As a result, the individual UE will have a beam produced in their particular direction, reducing interference and increasing capacity.

In summary, MIMO, is an antenna technology that uses multiple antennas at the transmitter and receiver ends to enhance data rates and signal quality for 4G LTE. With the help of spatial multiplexing, antenna diversity, and beamforming, MIMO improves both signal quality and bit rate.

1.2.2.2 Carrier Aggregation

In order to increase the channel bandwidth and subsequently the bit rate, carrier aggregation was introduced in LTE-Advanced. Component carriers (CC), are the names given to each aggregated carrier. The component carrier can be aggregated with a maximum of five component carriers, resulting in an aggregated bandwidth of 100 MHz. The component carrier can have a bandwidth of 1.4, 3, 5, 10, 15 or 20 MHz. There are numerous ways to aggregate the component carriers, but the simplest way is to group contiguous component carriers in the same band, a process known as intra-band contiguous aggregation. Separate carriers can be chosen in cases when this isn't a possibility. Figure 1.5 illustrates how they can come from the same band (intra-band non-contiguous carrier aggregation), but have gap or gaps in between or they may aggregate from separate band (inter-band carrier aggregation).

1.2.3 An evolution toward 5G

Technologies beyond the fourth generation (4G) have being explored as it has become a commercial success. Release 13 and Release 14 have been introduced as the bridge from 4G to 5G. Compared to LTE-Advanced, in Release 13 a significant number of new features have been introduced. The opportunistic use of unlicensed spectrum is developing into a key addition to satisfy the increasing traffic demand, even as licensed spectrum continues to be 3GPP operators' top priority for delivering enhanced services and user experience. Operators will have the opportunity to employ unlicensed spectrum with a unified network thanks to licensed-assisted access. In LTE, carrier aggregation was only possible with up to 5 component carriers (CC), but with this release, 32 CCs could be aggregated, increasing data rates and making it easier to combine several CC from different bands. Release 13 significantly enhances cellular network support for Machine-Type Communications (MTC) and the Internet of Things (IoT). Full Dimension MIMO (FD-MIMO), which increases the number of antenna from 8 to 64, has also been introduced. V2X, a new class of services, is one of the new ones added in Release 14. Reduced latency is the primary objective of this standard. Given that emerging applications like IoT and V2X require low latency, LTE offers latency of less than 10 ms. However,

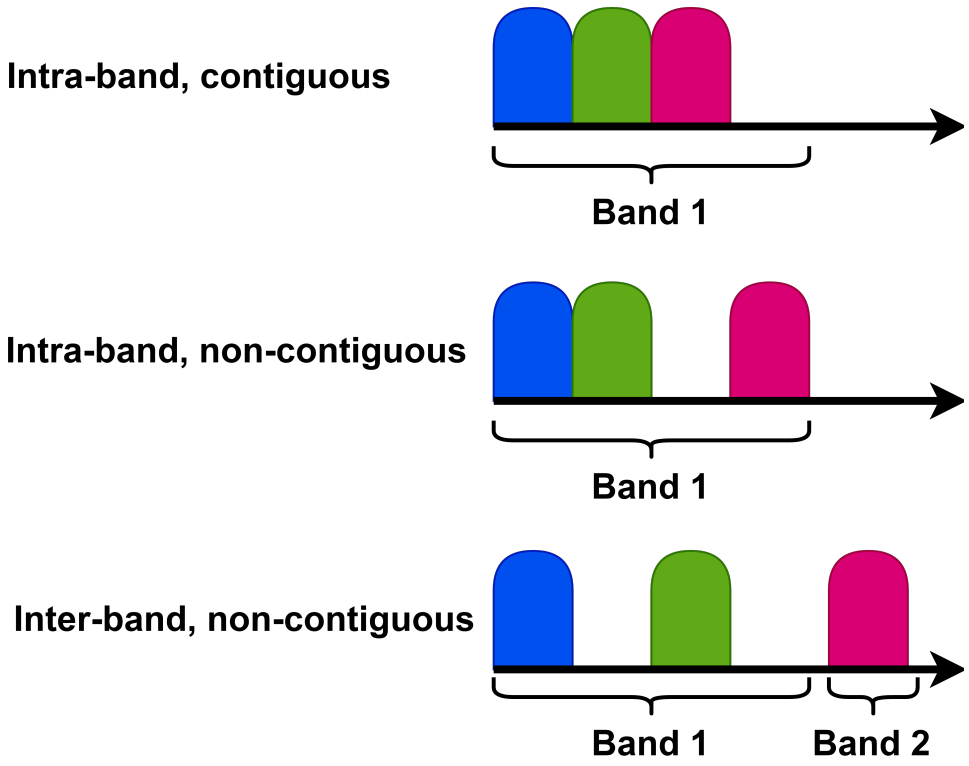

Figure 1.5: Schematic representation of carrier aggregation

1 ms over-the-air latency has been deemed to be a crucial requirement of 5G communication systems [10].

1.2.4 5G

Recent releases of the 3GPP protocol have expanded its services to include fields like Machine Type Communication (MTC), Device-to-Device (D2D), and Vehicle Communication (V2X). These already offered services are expected to be improved by 5G, which will also expand the range of services provided to include augmented reality, digital TV, public safety, and drone communication [11]. Two frequency ranges have been established by the 3GPP in Release 15: Frequency range 1 (FR1) [12], which covers the range from 410MHz to 7.125GHz, and Frequency range 2 (FR2) [13], which covers the range from 24.25 to 52.6GHz. In comparison to 4G, the channel bandwidth has been enhanced up to 100MHz. While FR2, which operates in the mm-

wave frequency spectrum, has a channel bandwidth of 400MHz that may be increased by carrier aggregation to reach the GHz range.
Moving to mmWaves is difficult because small-wavelength waves attenuate more quickly, for example because of atmospheric conditions. However, smaller antenna array components can be arranged closely together due to shorter wavelengths. In the mmWave spectrum, it is practical to create antenna arrays of tens or even hundreds of antenna elements. In addition to compensating for the increased losses suffered by mmWaves, this method produces antenna systems with high antenna gains and narrow beams that may also reduce interference due to their narrow beams.

1.3 Example of Requirements

This section includes some of the key requirements specified by the mobile standards as well as some quantitative examples from the most recent Releases. The RF receiver sensitivity and adjacent channel selectivity have been given special consideration.

1.3.1 Sensitivity

Wireless standards specify a reference sensitivity power level (REFSENS) that must be transmitted to the two antenna ports in order to ensure that the throughput meets the specified criteria for the expected modulation and coding scheme, known to as the reference channel. For example, in 3GPP Release 15 [13], specifications are given for reference channels with low SNR that use QPSK modulation and a 1/6 coding rate. In this scenario, sensitivity is needed to guarantee a throughput of 95% of the maximum achievable, which translates to an SNR of -2.6dB. For each band and each permitted carrier bandwidth, sensitivity is described in the standard. The sensitivity necessary for power class 3 is shown in table 1.1. For instance, by using a 100MHz bandwidth with

Operating band	**REFSENS (dBm) / Channel bandwidth**			
	50 MHz	**100 MHz**	**200 MHz**	**400 MHz**
n257	-88.3	-85.3	-82.3	-79.3
n258	-88.3	-85.3	-82.3	-79.3
n260	-85.7	-82.7	-79.7	-76.7
n261	-88.3	-85.3	-82.3	-79.3

Table 1.1: Reference sensitivity for power class 1

the n257 band and replacing the sensitivity value in 1.1, the necessary NF could be derived, leading to:

$$P_{sens[dBm]} = -85.3 = -173.8 + NF_{[dB]} + (-2.6) + 10log_{10}(100MHz) + IM_{[dB]}, \tag{1.10}$$

the IM, or implementation margin, which stands for "implementation margin", is expected to be 2.5 dB in this testing condition and accounts for any non-idealities that can affect signal processing before the demodulator. Consequently, the NF needed to pass the test is 8.6dB.

1.3.2 Adjacent channel sectivity

Adjacent channel selectivity (ACS) quantifies the receiver's ability to receive the desired signal in the desired channel, in the presence of an adjacent channel signal at a given frequency offset from the frequency of the desired channel, without degrading receiver performance. The receiver must meet the minimum specifications defined in a given standard. Tables 1.2 and 1.3, for example, show the specifications set forth for ACS for the FR1 and mmWave bands, respectively.

RX parameter	**Channel bandwidth**				
	10 MHz	**15 MHz**	**20 MHz**	**40 MHz**	**50 MHz**
ACS [dB]	33	33	33	33	33
RX parameter	**Channel bandwidth**				
	60 MHz	**80 MHz**	**90 MHz**	**100 MHz**	
ACS [dB]	33	33	33	33	

Table 1.2: ACS for FR1 bands with $F_{DL} \geq 3300MHz$ and $F_{UL} \geq 3300MHz$

RX parameter	**Channel bandwidth**			
	50 MHz	**100 MHz**	**200 MHz**	**400 MHz**
ACS [dB] for band n257, n258, n261	23	23	23	23
ACS [dB] for band n260	22	22	22	22

Table 1.3: ACS for FR1 bands with $F_{DL} \geq 3300MHz$ and $F_{UL} \geq 3300MHz$

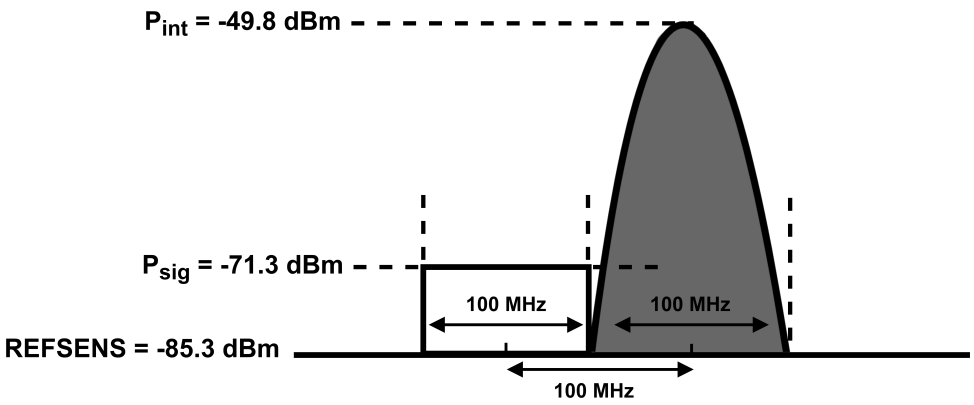

Figure 1.6: ACS test for Operating Band n257.

There are different test for ACS in the presence of an interferer on the adjacent channel. For bands in the FR1 and mmWave bands, these tests are different. However, in both cases, the desired signal is set 14 dB above REFSENS, and the interference has a variable amplitude depending on the carrier bandwidth. In the case of mmWave, the interferer power is set at 35.5 dB above REFSES for the n257, n258 and n258 operating bands, and at 34.5 dB above REFSENS for the n270 operating band. Figure 1.6 illustrates the situation for the operating band n257 with a channel bandwidth of 100MHz as an example. This needs to be tested using an interferer with the same bandwidth and 35.5 dB more power than the REFSENS (-85.3dBm).

1.3.3 Specifications for 5G Receiver

The sensitivity and selectivity specifications for a general 5G receiver have previously been defined. The receiver discussed in this thesis (chapter 3) has more exacting requirements than other receivers, not just in terms of noise and selectivity but also in terms of linearity, matching, and gain configuration. Table 1.4 lists the specifications for the receiver. The proposed receiver must support RF channel bandwidths ranging from 50 MHz to 2 GHz with a carrier frequency of 7 GHz. The receiver's gain should be programmable down to 0 dB, with a maximum gain of 45 dB. In all gain settings, the receiver should be able to achieve +15 dBm of IP3 at the output of the receiver. It should have a noise figure of less than 5 dB, and for every dB of gain reduction, the noise figure shouldn't rise by more than 0.7 dB.

Item	Condition	Specs	Unit
Carrier Frequency		7000	MHz
RF Channel BW	Mode (50,100,400, 400, 800, 1600 and 2000)		MHz
Input VSWR	in all modes	1.5	
Gain Control Range	Max Gain	45	dB
	Min Gain	0	dB
Noise Figure	@LNA input, max gain	5	dB
Noise Figure Slope		0.7	dB/dB
Input P1dB	Max Gain, inband	-39	dBm
Input P1dB	Min Gain, inband	6	dBm
OIP3	All gain step, $P_{RxOUT} = -8dBm$	>15	dBm
Analog Filter Selectivity	From Bandwidth to 4 x bandwdith	-33	dB
In-band Flatness	in all modes	1	dB
Power Consumption	Max gain, Max BW		mW

Table 1.4: The Specification of the Receiver.

1.3.4 Conclusion

This chapter provided an overview of the key wireless standard requirements as well as a discussion of how mobile networks have evolved. It should be obvious at this time that the trend is toward faster speeds, multiple bands, multiple antennas, and greater carrier bandwidths. Several bands and antennas make it highly desirable to have receivers that can function over multiple bands, which eliminates the need for extra RF filters and duplexers. This suggests a number of difficulties, particularly in terms of linearity. This problem is reflected in the baseband receiver design, which is often a Trans-Impedance Amplifier (TIA). A highly linear TIA design with large bandwidth will be shown in the following chapter.

Chapter 2

Design of Highly Linear TIA with 1.5 GHz of BW

Abstract
As previously said, the design of the baseband has become more difficult due to new wireless standards. One of the key reasons is that, when carrier aggregation is taken into account, the bandwidth may approach the GHz range. The operational transconductance amplifier (OTA), whose unity gain frequency impacts the accuracy of the transfer function and distortion, sets a restriction on the maximum bandwidth of a closed loop filter. Both of these concerns are influenced by the OTA gain vs. frequency relationship, thus it should be maximized up to the filter band-edge and maintained at a sufficiently high up to the frequency of the furthest blocker.
In this chapter a trans-impedance amplifier closed in feedback with a shunted R-C will be presented. In order to support both 5G and future wireless standards it has a programmable bandwidth up to 1.5 GHz. Feedforward compensation together with inductive peaking is used to ensure stabilization.

2.1 General Consideration

High linearity, very little noise, and low power consumption are all requirements for baseband filters. As previously mentioned, as RF frequencies increase, it becomes more difficult to meet these requirements. Either a trans-impedance amplifier (TIA) filtering or higher order filter makes up the first block in the widely used current-mode receiver architecture following the mixer [14]. In addition to the requirements mentioned above, baseband must ensure low input impedance up to very high frequencies in order to preserve

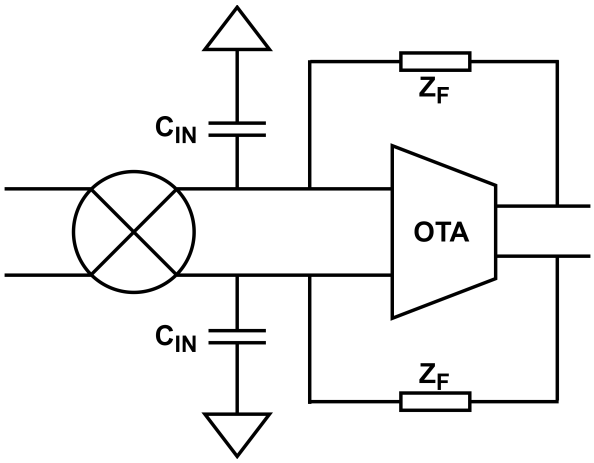

Figure 2.1: Closed Loop TIA with big Input Capacitor.

the RX front-end's linearity. Operational Transconductance Amplifier (OTA) closed in loop is the base for TIA implementation. Since the TIA's input impedance increases as gain decreases, which happens as frequency increases, A large shunt capacitance is connected to the TIA's virtual ground node to provide a low impedance path for high frequency components in order to address this problem, as shown in the figure 2.1. When there are strong OOB interferers present, this capacitor preserves the front-end IIP3 by providing low input impedance [15] and filters down converted interferers to improve TIA OOB IIP3.

The issue with such a large capacitor is that the noise performance degrades. This capacitor could be of the order of pF as in [16] and [17]. Let's consider the figure 2.2, where the input referred voltage noise source is shown. By computing the noise transfer function (NTF) to the TIA output, the following result is obtained:

$$NTF = \frac{\overline{V_{n,OUT}^2}}{\overline{V_{n,IN}^2}} = \left|1 + \frac{Z_F}{Z_D}\right|^2. \tag{2.1}$$

where Z_D is the driving impedance and Z_F is the impedance of the feedback network, as shown in figure 2.2. When Z_F is assumed to be parallel of RF and

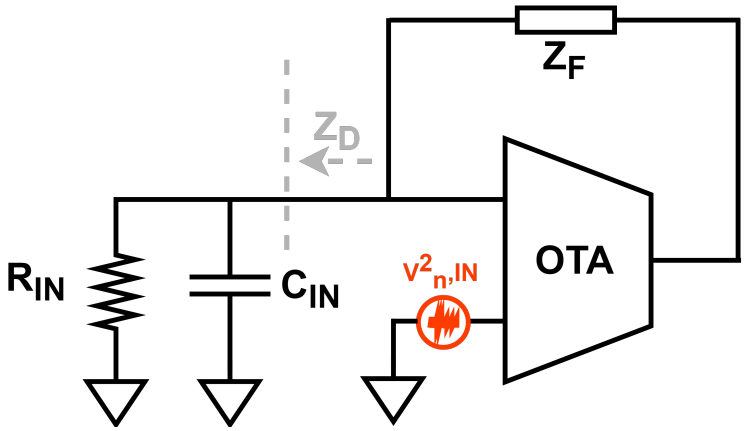

Figure 2.2: Schematic representation of TIA with input referred voltage noise source.

CF, 2.1 transforms to the following:

$$NTF = \left|\frac{R_{IN}+R_F}{R_{IN}}\right|^2 \left|\frac{1+s\dfrac{C_{IN}R_FR_{IN}}{R_F+R_{IN}}}{1+sC_FR_F}\right|^2 \tag{2.2}$$

It is evident from equation 2.2 that NTF has a zero, which is given by the expression $\omega_Z = 1/(C_{IN}(R_D||R_F))$, which becomes $\omega_Z \approx 1/(C_{IN}R_D)$ in the event that $R_F >> R_D$. As C_{IN} increases, ω_Z shifts to lower frequencies, which worsens the TIA's in-band noise. This condition is depicted in figure 2.3 where it compares the output noise of TIA vs. C_{IN}. In this illustration, the cut-off frequency of TIA is set to 1.5 GHz, and R_{IN} is selected to be 100 Ohm. When 1pF is used, C_{IN} results in a zero at $\omega_z = \omega_0$ in the NTF. Beyond this C_{IN} value, however, the integrated noise increases with the square of C_{IN} and becomes unacceptable. A 2^{nd} order open loop filter is placed in front of the TIA as the proposed solution. Low input impedance should be guaranteed by the TIA in order to ensure strong linearity for an expanded frequency range of the open loop filter. The OTA must have a high loop gain up to GHz of frequency range and low power consumption in order to meet this requirement.

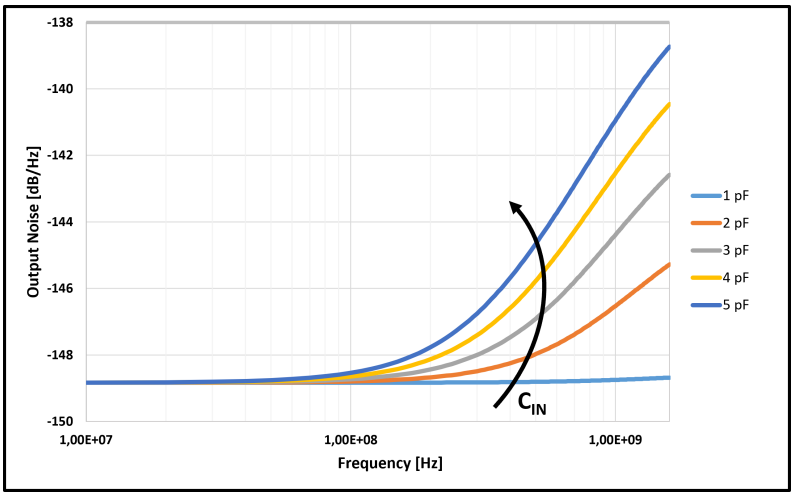

Figure 2.3: Output noise of TIA vs. C_{IN}.

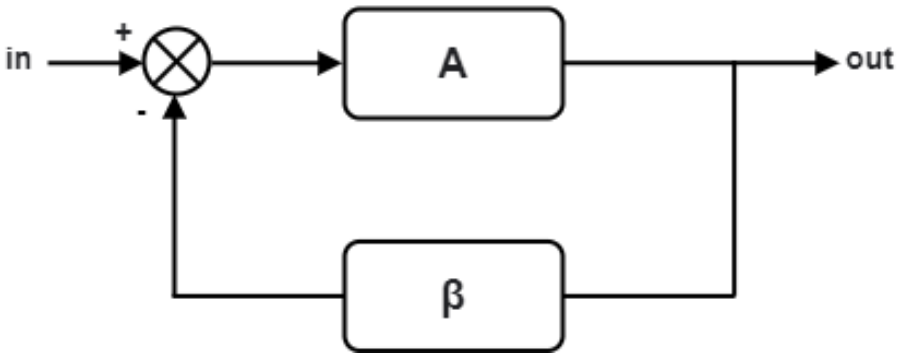

Figure 2.4: Negative Feedback system.

2.1.1 Stability in Feedback System

As with any feedback system, stability is a crucial consideration in circuit design, especially when the bandwidth is as wide as it is in this case. If nothing is done, the circuit can become unstable and stop working as it should. Intuitively, the instability is caused by the excessive phase shift of the element present in the loop. Above a certain frequency, this excessive phase shift puts the circuit into positive feedback, which causes instability.
The needed unity gain frequency with GHz of bandwidth makes challenging the stabilizing of the amplifier.
Consider a general negative feedback system as shown in figure 2.4, the closed

loop transfer function can be expressed as follows:

$$G(s) = \frac{A(s)}{1 + \beta A(s)}, \tag{2.3}$$

The amplifier's open-loop gain is represented by the quantity $A\beta$; if $A\beta$ is significantly higher than 1, the feedback network β alone decides total transfer function in the equation 2.1. It should be noted that 2.1 goes to infinity if $\beta A(s = j\omega) = -1$. The circuit can boost its own noise up to the point when it starts to oscillate. Alternatively said, the circuit might oscillate at frequency ω_1. As a result, the condition in which the circuit may oscillate can be written as follows:

$$\begin{aligned} &|\beta H(j\omega_1)| = 1, \\ &\angle\beta H(j\omega_1) = -180^\circ. \end{aligned} \tag{2.4}$$

The 2.4 is called "Barkhausen's criteria". Since the negative feedback adds an additional 180° phase shift, the total phase shift is now 360°. This transforms the feedback into a positive one causing instability. Therefore, the total phase shift for $\beta A = 1$ should be more positive than -180° to prevent instability.

2.2 Design of TIA

As shown by figure 2.5, the proposed TIA is based on an operational transconductance amplifier (OTA) with a parallel R-C feedback network. The implemented TIA should have a bandwidth of up to GHz, requiring several GHz of unity gain bandwidth for the OTA. Additionally, the TIA should have excellent linearity, which means the OTA needs a high loop gain for a wide frequency range. In essence, there are two techniques to increase the gain of the OTA: cascading, which involves utilizing a multi-stage amplifier, and cascoding, which means stacking more transistors on top of one another in a single-stage amplifier to increase the output resistance, which increases the gain. Cascoding is very challenging in low voltage environments. Since stacking additional transistors reduces the voltage headroom available for transistors to operate in the proper biasing condition in the presence of a significant output swing of the signal. Therefore, using a multi-stage amplifier is the only way to increase the gain. The main disadvantage of this approach is that it causes an extra phase shift in the frequency response since each stage of the cascade acts as a capacitive load for the previous stage. Therefore, frequency compensation is crucial when using a multi-stage amplifier.
In this work, an unconventional Feed-Forward architecture has been used to

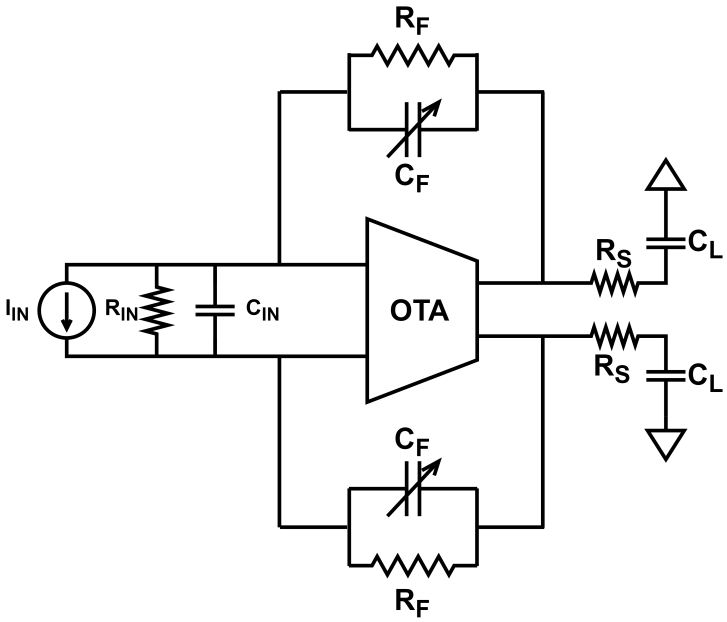

Figure 2.5: The Schematic representation of the proposed TIA.

implement an OTA with three stages, and inductive peaking has been used to guarantee stabilization [18] [19], as illustrated in figure 2.6.

2.3 Design of OTA

As mentioned above, the OTA was designed using an unconventional feedforward topology, as illustrated in figure 2.6, in order to achieve wide bandwidth and ensure loop stability over a broad frequency range.

2.3.1 FeedForward Topology

As was already mentioned, OTA with three stages has been used in this work. Stability issues arise due to the phase shifts introduced by each additional stage. There have been numerous compensating methods for multi-stage amplifiers documented in the literature [20]. The most traditional one employs pole splitting (Miller effect) to increase the non-dominant pole's frequency while pulling back the dominant pole to a sufficiently low frequency. However, this restricts the bandwidth that may be employed, particularly for a large capacitive load, unless very high power consumption is used in the output

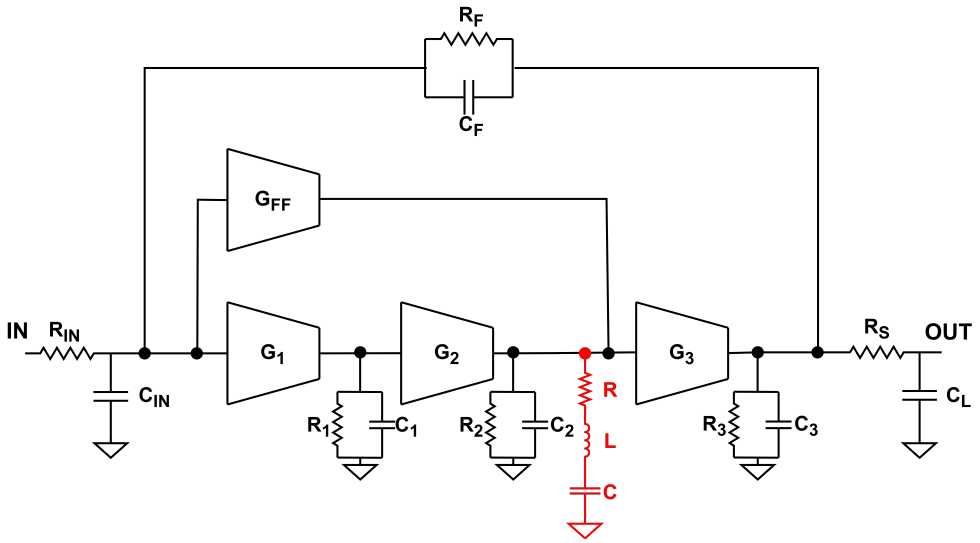

Figure 2.6: The Schematic representation of the OTA with inductive peaking.

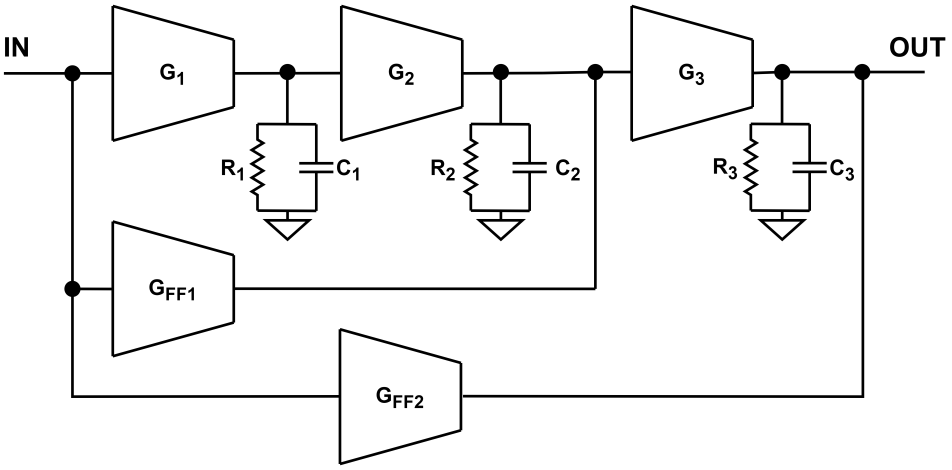

Figure 2.7: The Block Diagram of FF Topology.

stage to force the second pole out sufficiently. Additionally, the possible gain at frequency near to the UGBW is constrained by the -20dB per decade form of the frequency response.
The feedforward topology is a topology that can achieve high gain at high frequency and ensure stability even for a very large UGBW.
In general, the number of FF path needed to introduce the necessary zeros to

ensure stability is equal to the number of stages in the main path minus one, as shown in figure 2.7. A fifth order structure using this topology was used to build a continuous-time sigma-delta ADC sampled at 8 GHz using 28 nm CMOS technology [21]. The amplifier used in the integrators has a unity gain frequency of 6.7 GHz and a gain of 28 dB at 1 GHz, however it consumes more than 135 mW. The bottom FF stage dissipates a substantial amount of the power (40 mW). In order to ensure rail to rail output swing, this stage needs an extremely high gm and cannot benefit from current re-use through element stacking. The topology proposed employs a third order FF topology, shown in figure 2.8, and eliminates the outer FF path of figure 2.7. The FF path defines the unity gain frequency and phase margin, while the main path provides the most of the gain. In order to avoid limiting of the output swing, the FF path is connected from the OTA input to the input of the last stage. Compared to the outer FF stage in figure 2.7, this topology uses less power.
Assume that the main path has three stages with DC gains A_1, A_2, and A_3 each introducing a pole at $\omega_{P1} = 1/R_1C_1$, $\omega_{P2} = 1/R_2C_2$ and $\omega_{P3} = 1/R_3C_3$, respectively. The FF stage, on the other hand, has a DC gain A_{FF} and shares $\omega_{P2} = 1/R_2C_2$ with the second stage. The transfer function can be easily calculated and is expressed as follows:

$$TF(s) = \frac{(A_1\,A_2\,+\,A_{FF})\,\left(1\,+\,\frac{A_{FF}\,s}{(A_1\,A_2\,+\,A_{FF})\,s}\right)A_3}{(1\,+\,s/\omega_{P1})\,(1\,+\,s/\omega_{P2})\,(1\,+\,s/\omega_{P3})}. \tag{2.5}$$

The position of the zero that the FF path introduces can be calculated using the 2.5:

$$\omega_{Z1} = -\omega_{P1}\left(1 + \frac{A_1A_2}{A_{FF}}\right) \approx -\frac{gm_1}{C_1}\frac{gm_2}{gm_{FF}}. \tag{2.6}$$

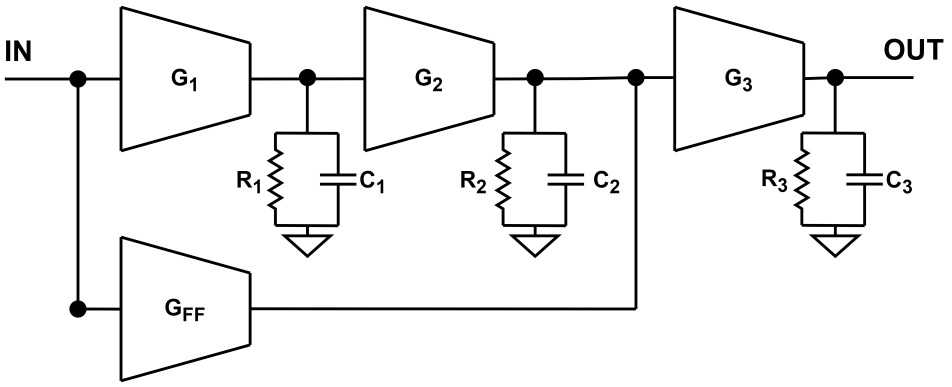

Figure 2.8: The Block Diagram of The Proposed FF Topology.

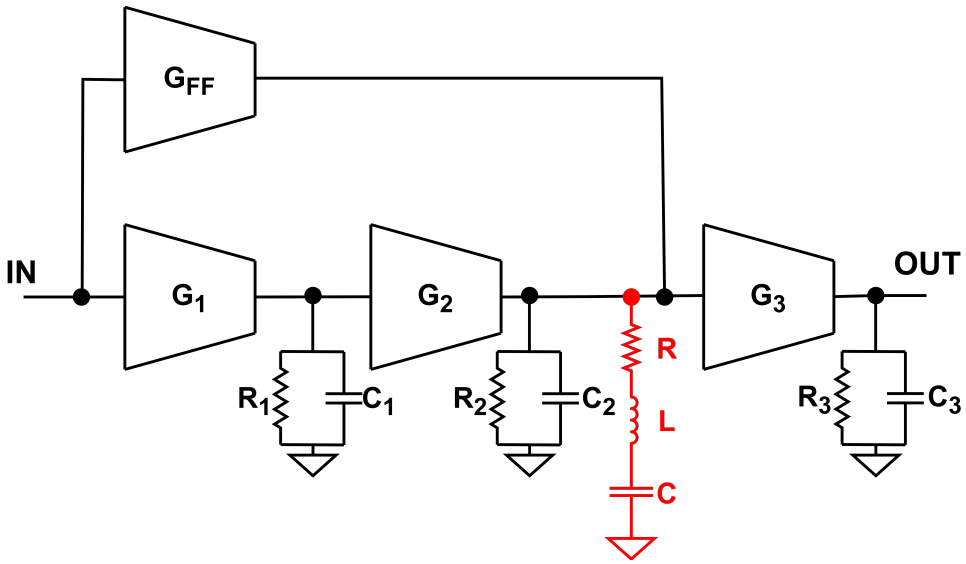

Figure 2.9: The Block Diagram of The OTA with Passive Zero.

According to 2.6, the location of the zero is approximately equal to α times the GBW product of the first stage, where α is the ratio of the second stage's to the FF stage's transconductance. It is also obvious that there will be a trade-off between the power consumption and the possible UGBW as the location of the zero increases correspondingly to the product of the first and second stage's transconductance. Since there are three stages in the main path, which correspond to three poles, and only one zero is introduced by the FF stage, there may still be stability problems. There are two ways to solve this problem: the first is to move the pole associated to the second and FF stage beyond the unity gain frequency (ω_u), and the second is to add another zero. The first option is not feasible because, in order to move beyond ω_u, output resistance must be very low, which causes the OTA gain to drop to an unacceptable level. As a result, the second method is used, passively producing the zero while maintaining gain and saving power, as shown in figure 2.9. In addition, using inductive peaking improves the unity gain bandwidth.
The relationship between ω_u and the zero determines the stability of the op-amp. Since ω_u is approximately equal to $\frac{gm_{FF}Rgm_3}{C_L}$ in the first order, As a result, the ratio is $\frac{\omega_u}{\omega_Z} = \frac{gm_{FF}}{gm_1}\frac{gm_3}{gm_2}\frac{C_1}{C_L}gm_{FF}R$. Given that the other terms in this expression can be precisely controlled, $gm_{FF}R$ is crucial. A replica circuit could be used to adjust the bias current that results in the right $gm_{FF}R$ in order to solve this problem.

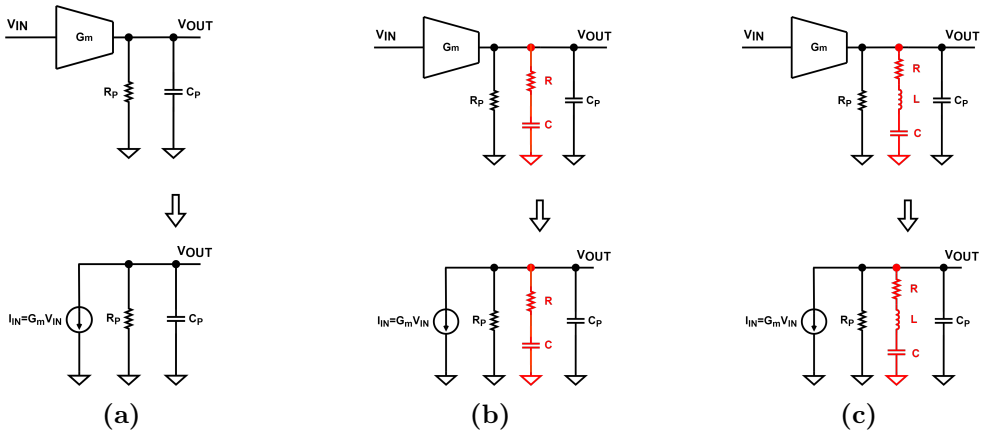

Figure 2.10: Three simplified circuits to explain the different output loads of the FF/second stage: (a)Output load with the MOSFET's parasitic output resistance and capacitance; (b) output load with a zero cretaed by R and C; (c) output load employing inductive peaking.

2.3.1.1 Passive zero creation with Inductive Peaking technique

In order to comprehend the advantage of the inductive peaking method. Consider the scenario in figure 2.10a, where there is no load adjustment. Figure 2.11 illustrates the transfer function of the FF stage in this scenario. As can be seen, the phase shift causes a poor phase margin (24°). As previously said, moving the pole associated to the second and FF stage beyond ω_u will improve the phase margin. This may be accomplished by placing a small resistance in parallel, but doing so reduces the overall gain of OTA [Fig.2.11]. A capacitor in series with the resistor might be added, as illustrated in figure 2.10b, to maintain gain up to the frequency of interest. The phase margin, as illustrated in figure 2.11, is improved by this method and it becomes 48°.
Inductive peaking is utilized to reduce the phase margin to a level acceptable [Fig.2.10c]. For $\frac{V_{OUT}}{V_{IN}}$, the inductive peaking technique provides a transfer function of third order. However, given that C is more than ten times larger than C_{Par}, it is plausible to suppose that C can be replaced by a short circuit close to ω_u, leading to the following simplified transfer function:

$$\frac{V_{OUT}}{V_{IN}}(s) = -G_m \frac{R_{Par}(R+sL)}{(R+R_{Par})+s(C_{Par}R_{Par}R+L)+s^2LC_{Par}R_{Par}}. \quad (2.7)$$

Figure 2.11 illustrates how the $R||RP-CP$ pole causes a 35-degree phase shift around ω_u in the absence of an inductor (L). A $1.2nH$ inductor has the effect

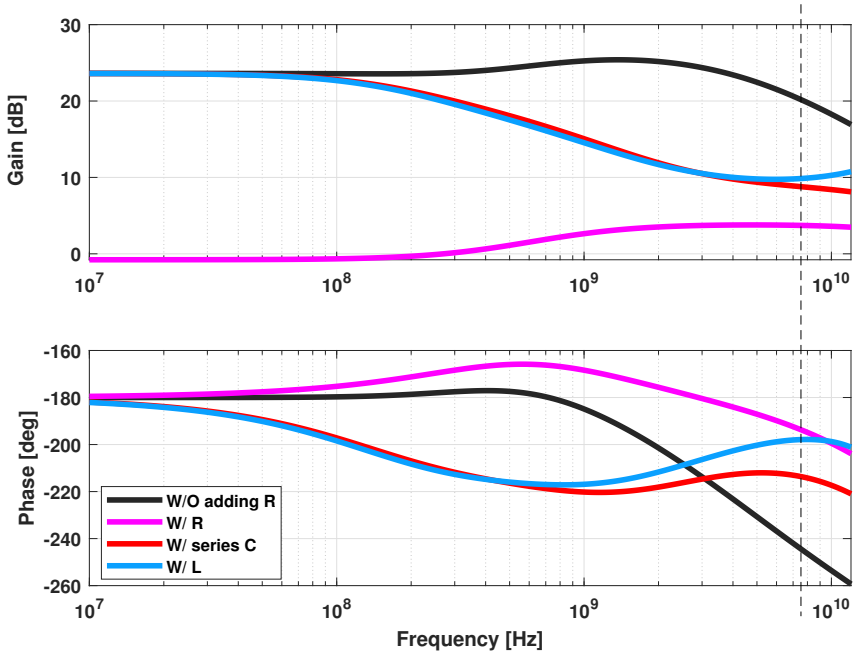

Figure 2.11: The Effect of Inductive Peaking technique on the transfer function of the FF stage.

of causing the phase to change more slowly before the resonant frequency but more quickly after. This leads ω_u to grow by $1GHz$ (from 6.5 to 7.5 GHz), and it also produces a 19° phase shift around ω_u (i.e. 7.5 GHz).
The area is the problem with employing an inductor. Generally, the area is influenced by the inductance value, which is connected to the position of the zero and, eventually, to the desired UGBW. Smaller area is achieved, constructively coupling the two differential inductors to maximize their resulting value, as shown in figure 2.12. Additionally, since a high quality factor is not necessary, narrow windings are used. The inductor dominates the OTA area in the situation under consideration. However, as the UGBW is extended, the inductor area will decrease and the benefits of increased bandwidth will be even higher.

2.3.2 OTA Design

The OTA is designed using a third order FF architecture, whose complete schematic is shown in figure 2.13, to achieve high loop gain and preserve good

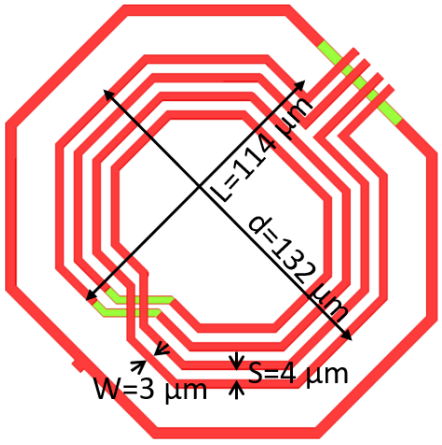

Figure 2.12: Layout of Coupled Inductors.

linearity.
The first stage is a high gm class A complementary p-n structure. The transistor sizes are selected to bias in a deep sub-threshold region, so as to have a high gm/I ratio. For a high DC gain, the input differential pairs are cascoded. Its small signal voltage gain is equal to the output impedance times the transconductance (gm) of the input transistors M_1^1 and M_4^1. Consequently, the expression for small signal voltage gain is:

$$A_v = (gm_1 + gm_4)\, R_{out}, \tag{2.8}$$

where R_{out} is the parallel of $gm_2\, R_{ds,2}\, R_{ds,1}$ and $gm_3\, R_{ds,3}\, R_{ds,4}$.

Class-AB low-gain wideband amplifier makes up the second stage. A class AB behavior is required because, in the event of a large signal present at the band edge or, or even worse, outside the band, such as a large current at 4 GHz, the last stage should be able to absorb the current even if the signal swing is filtered out since it is outside the band. At the output of the second stage, a class AB behavior is required in order to avoid entering into slewing and preventing early compression because a certain voltage swing is required at the input of the last stage in order to absorb large current.
By considering that Node 1 behaves as ground for differential signals, its operational principle can be understood. The output resistance multiplied by the sum of the M_2^2 and M_3^2 transconductances results in the small signal voltage

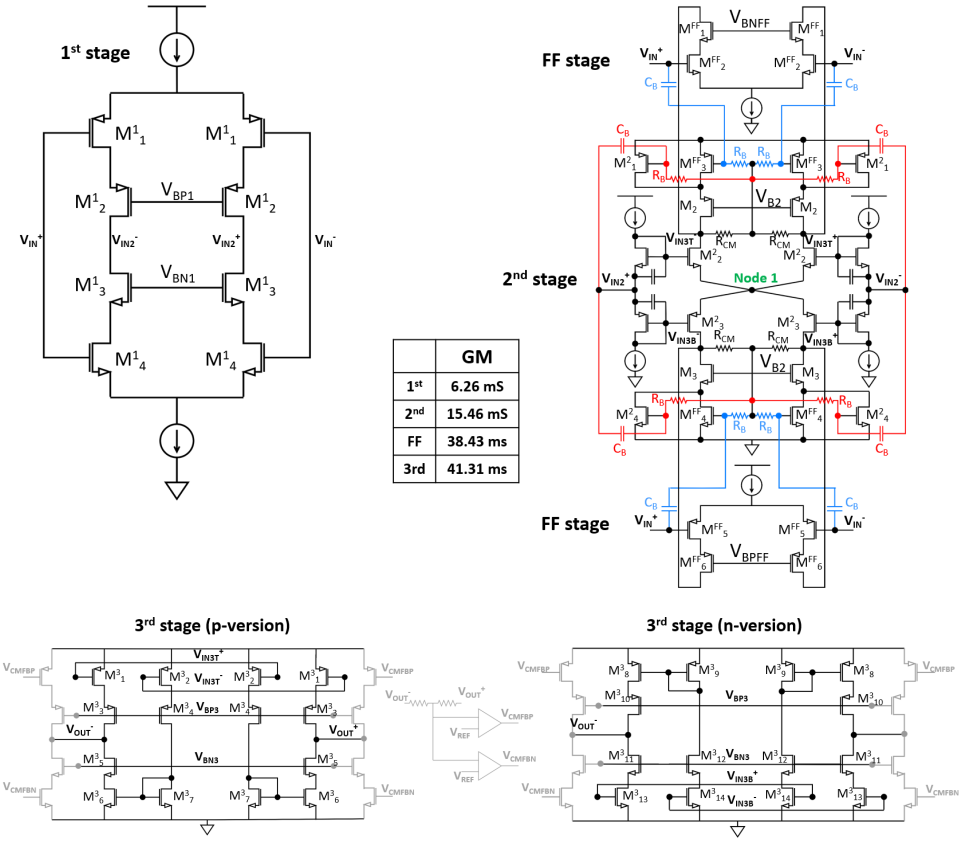

Figure 2.13: The Complete Schematic of OTA.

gain. It can be expresses in the following way:

$$A_v = (gm_2 + gm_3)\,(R_{outT}||R_{outB})\,, \tag{2.9}$$

where $R_{outT}(R_{outB})$ is the parallel combination of the resistance seen by the drain of M_2^2 and M_2 (M_3^2 and M_3).
A boosting capacitor is placed between the input and the gate of the load transistor at the section of the schematic that is highlighted in red. Intuitively, as the frequency increases, C_B turns into a short circuit and feeds the input signal to the load transistor as well, taking use of the load transistor's transconductance. This results in a multiplication of the total equivalent gm by about a factor of two. This increases the phase margin and expands the bandwidth by

creating a zero-pole doublet separated by an octave.

$$\omega_Z = \frac{1}{C_B R_B \left(1 + \frac{gm_1^2}{gm_2^2}\right)} \quad and \quad \omega_P = \frac{1}{C_B R_B}. \tag{2.10}$$

Two resistors (R_{CM}), each with a value of $50k\Omega$, are connected between the output node and the gate of the load transistors (M_1^2 and M_4^2) to provide the common mode feedback (CMFB). Large resistance was chosen because, for differential signals, these two resistances appear parallel to the output node's resistance; otherwise, choosing a small value would result in a small voltage gain.

The second stage has two differential outputs, one at the drain of the p-mos load transistors and the other at the drain of the n-mos load transistors, as illustrated in figure 2.13. Conceptually, the FF stage might also make use of p-n stacking (i.e. M_2^{FF} and M_5^{FF} could be stacked). If the input transistors are not cascaded, the large biasing current would reduce the gain of the second stage. Due to supply voltage limitation, cascoding translating into using two parallel FF stages, one with n-mos and the other with p-mos input transistors. Even in the FF stage, the boosting capacitor (CB) has been included (drawn in blue); in this instance, the load transistors (M_3^{FF} and M_4^{FF}) are driven by the input of the OTA, as opposed to the second stage, where they are driven by the signal from the output of the first stage. The p-mos and n-mos load transistors of the second stage and of the FF stage are merged together and drive the complementary p-n push-pull output stage. Figure 2.14 shows the effect of the inductive peaking technique on the overall loop gain when compared to the solution using only R-C. This shows a phase margin improvement of almost 20 degrees.

The third stage, or last stage, is a class AB amplifier to maximize the output driving capacity. In order to connect them directly to the two outputs of the second/FF stage, two parallel class AB amplifiers have been implemented, one with n-mos input transistors and the other with p-mos input transistors, so as to have $4gm$ at output. Let's only take into consideration the design with n-mos input transistors in order to comprehend its operation principle. The transistors M_{13}^3 are controlled by the previous stage, whereas transistors M_8^3 are driven by a current mirror made up of transistors M_{14}^3 and M_9^3. The quiescent current of the class AB stage can be controlled very precisely, being set through a current mirror. Common mode feedback circuits are still necessary but only to compensate for the mismatches between the p-mos and n-mos

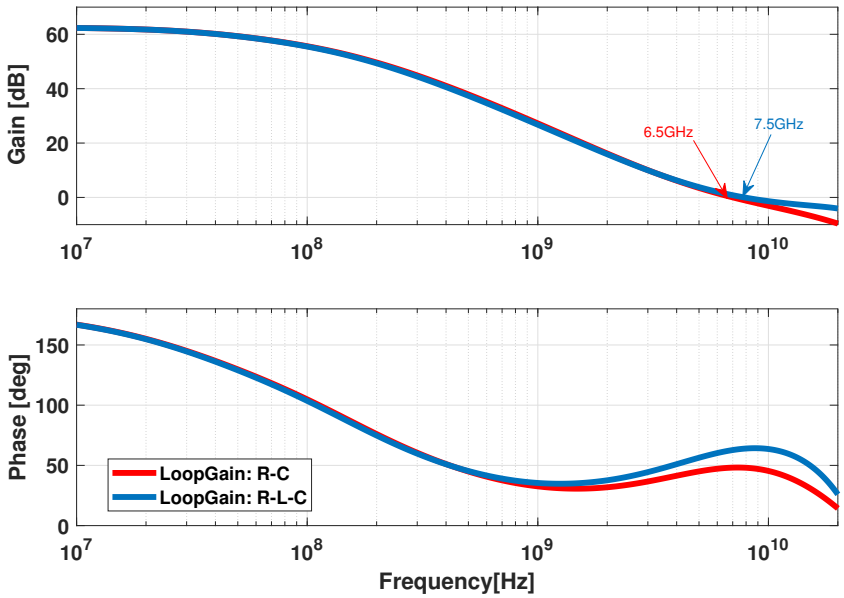

Figure 2.14: The Response of the Loop gain with R-C and with R-L-C.

current mirrors.
An extremely low common mode gain are the major benefit of implementing a n only (p only) output stage. This is crucial to stabilize the common mode response of the OTA, since the FF path is positive feedback for common mode signal.
The common mode voltage of the output nodes is set by the common mode feedback (CMFB) circuit of Figure 2.13 (Drawn in Gray). The output's common mode voltage is extracted using two identical resistors with values of $50k\Omega$, and it is then compared to a reference voltage of vdd/2. In order to reduce the error between the reference voltage and common mode voltage, the output of the CMFB amplifier regulates the current in the two branches of the output stage through the two generators controlled by V_{CMFBP} and V_{CMFBN}. The CMFB amplifire is implemented through a differential pair with differential-to-single-ended conversion.

2.3.3 TIA Stability

Figure 2.15 reports the implemented TIA. Even if the implemented version is fully differential, the single ended version is reported for simplicity's sake.

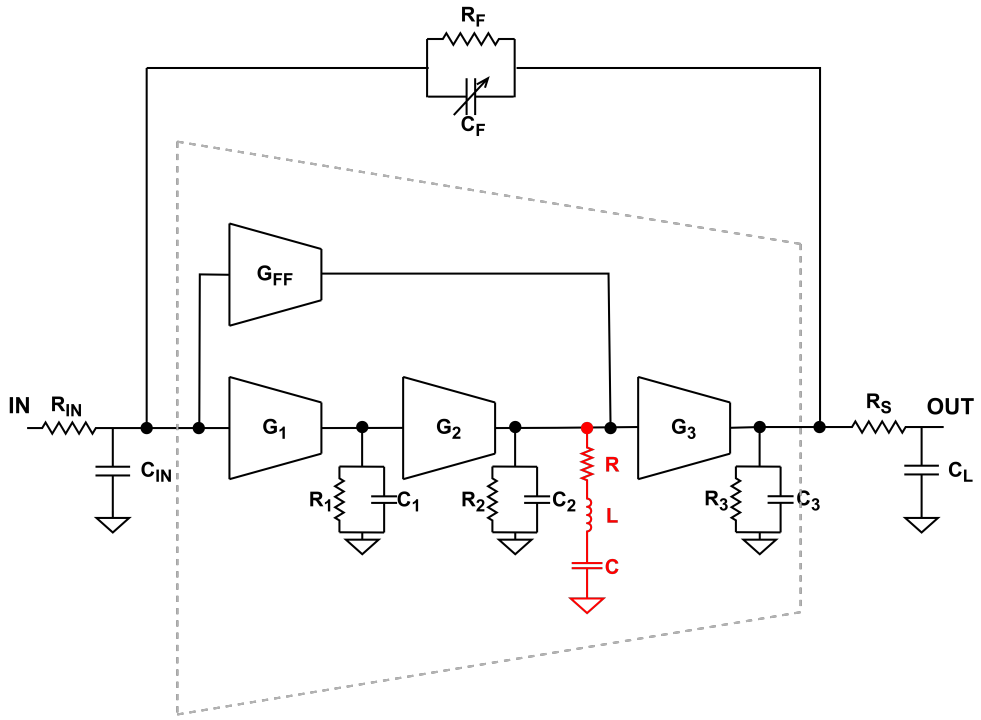

Figure 2.15: The implemented TIA.

Parameter	Value	Unit
R_{IN}	1	$k\Omega$
C_{IN}	90	fF
R_F	530	Ω
C_F	$180 - 530$	fF
C_L	500	fF
R_S	50	Ω

Table 2.1: The design parameter of the implemented TIA

Table 2.1 lists the value of passive components utilized in TIA. The cut-off frequency of the TIA is specifically determined by the values of R_F and C_F, and C_F is a tunable capacitor that is used to modify the TIA's closed loop bandwidth. As previously stated, R_{IN} and C_{IN} stand in for the driving impedance of the prior stage. While C_L represents the load capacitance, which represents

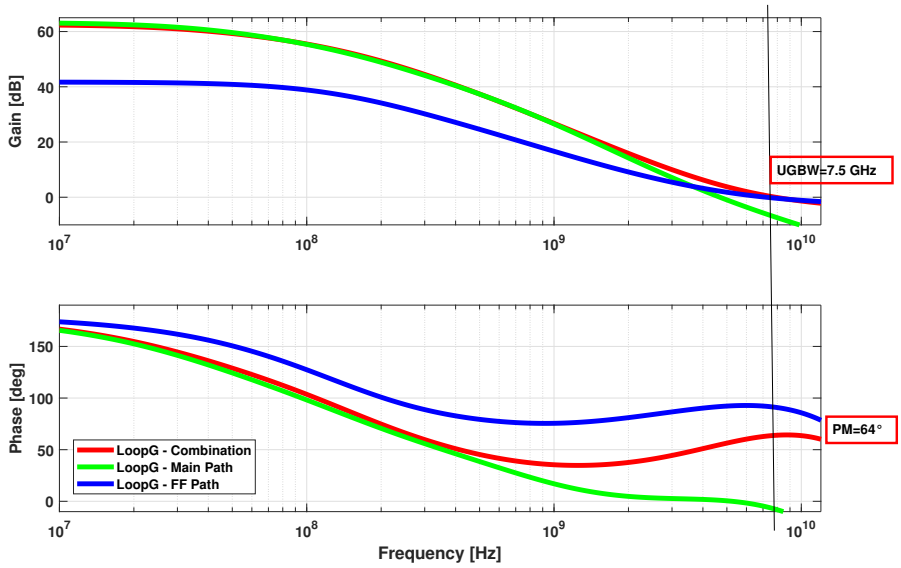

Figure 2.16: Loop gain of the TIA.

Corner	TT			SS			FF			SF			FS		
Temp. [C]	-50	27	100	-50	27	100	-50	27	100	-50	27	100	-50	27	100
UGBW [GHz]	11.7	7.5	5.7	16	10	6.7	7.9	6.2	5	10.5	6.9	5.3	13.3	8	6
PM [deg]	67.7	64	61	40	45	60	58	50	44	69	65.5	59.5	64.8	68	63

Table 2.2: TIA stability simulations results in PVT.

the next stage's input capacitance (i.e. ADC). A resistance (R_S) of 50Ω is placed in series with CL to provide a zero in the loop at around $6.5GHz$ in order to further improve the phase margin.
Figure 2.16 shows the overall loop gain. Figure[2.16] also shows the loop gains of the main path (shown in green), which is obtained by excluding the FF path, and the FF path, which is obtained by excluding the main path. It is obvious that the main path provides the gain up to the frequency of interest (i.e. 1GHz), as the main path dominates the loop gain at those frequencies. At higher frequencies, on the other hand, the FF path, which controls the UGBW and phase margin, dominates the loop gain.
With this solution, stability is guaranteed for temperature variations and process variations. The "SS corner" variation, which has a 45° phase margin, provides the worst-case scenario for nominal temperature.

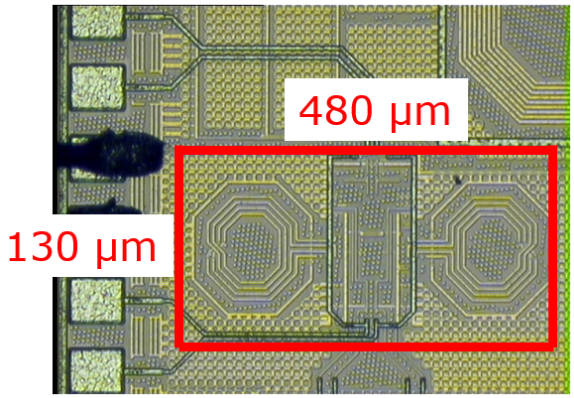

Figure 2.17: Chip micro-photograph.

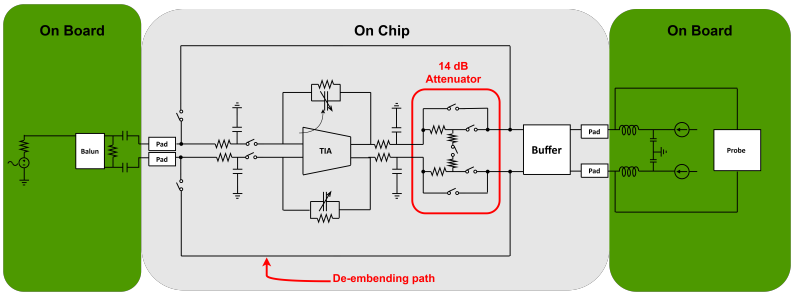

Figure 2.18: Measurement setup for the stand-alone TIA.

2.4 Measurement Results

The proposed TIA was implemented and tested as a stand-alone filter. Tsmc 28nm HPC CMOS technology was used to fabricate the prototype. The micro-photograph of the chip with an active region of $0.06mm^2$ is shown in figure 2.17.

In order to avoid the loading impact of bonding wires and PCB traces, an on-chip output buffer with 0-dB gain is implemented. For testing of linearity, a 14 dB resistors-divider attenuator is placed in front of the buffer. For measurements of transfer function and noise, the attenuator could be by-passed. Switches that are controlled from outside are used to set these various configurations. Figure 2.18 illustrates the setup for characterizing the TIA. The bare die is bonded to the PCB, and a 1:1 external balun was mounted there to transform the single-ended signal into a differential signal. R&S RT-ZD40 dif-

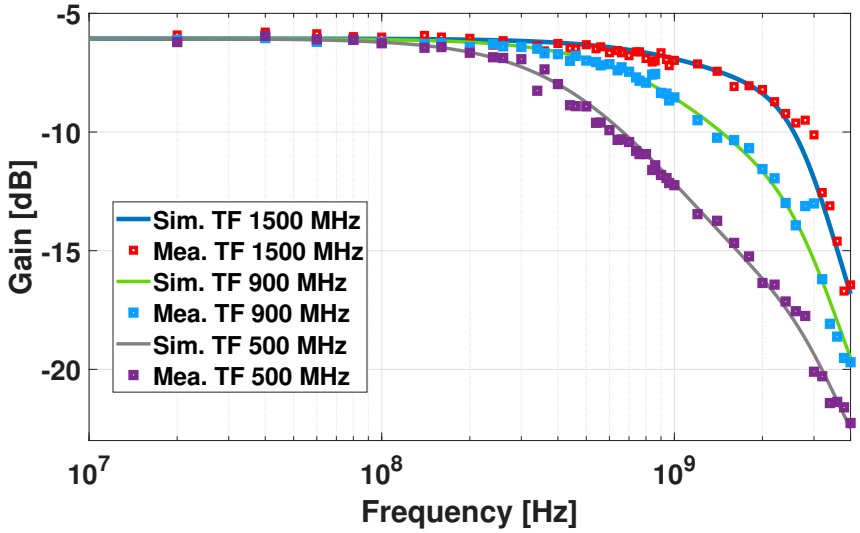

Figure 2.19: The transfer function for different bandwidth configuration.

ferential probe and R&S FSQ8 signal analyzer are used to detect the output. The TIA transfer function is shown in figure 2.19 and includes different cut-off frequencies (i.e. 1.5GHz, 900MHz, 500MHz). The correlation between measurements and simulations is good. While the simulations are getting closer on the measured bandwidth plot. As bandwidth is increased, higher out of band selectivity is sought after, even if the lower bandwidth plot approaches the desirable 1st order response. Due to the capacitance (C_L plus parasitic) in series with 50 ohm at 3 GHz, there is an additional pole.
Figure 2.20a shows simulated and measured IIP3 versus first tone position keeping the IM3 tone at $300MHz$. Reasonable agreement is obtained. An excellent In-band (IB) value ranging from 35 and $42dBm$ is obtained. In general, for a three-stage OTA typically, three sources of distortion dominate. Which are output conductance and transconductance of the last stage and the transcoductance of the first stage [22]. The first term depends on the output swing, which is frequency dependent, because as the frequency increases the voltage swing is reduced. The second term, which depends on the current absorbed by the last stage, is frequency independent. Since absorbing a large current results in a large voltage swing at the last stage input, this could also cause the intermediate stage to slew and produce more distortion. The third distortion depends on the voltage swing at input which depends on the input impedance. Since, as the frequency increases the loop gain decrease which

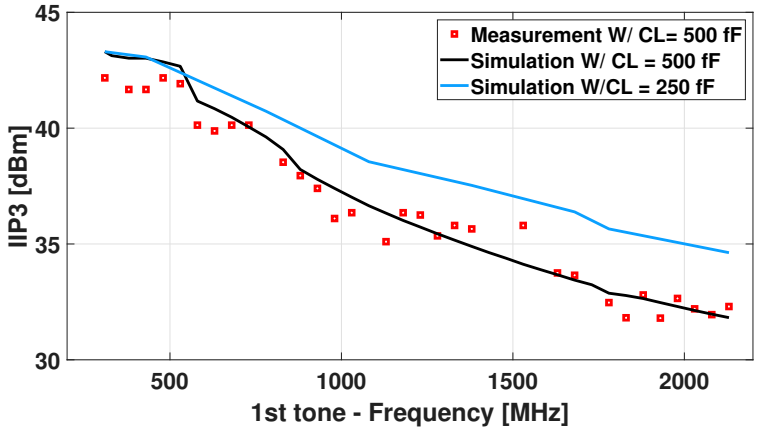

(a) IIP3 vs 1^{st} tone.

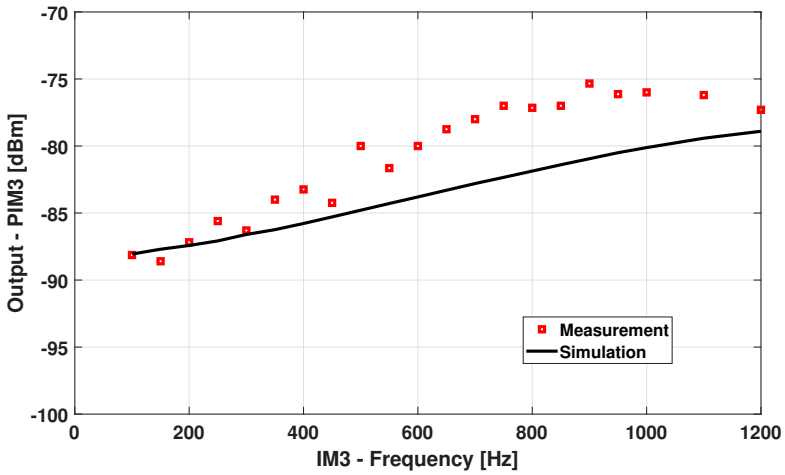

(b) Simulated and measured output IM3 as a function of IM3 frequency.

Figure 2.20

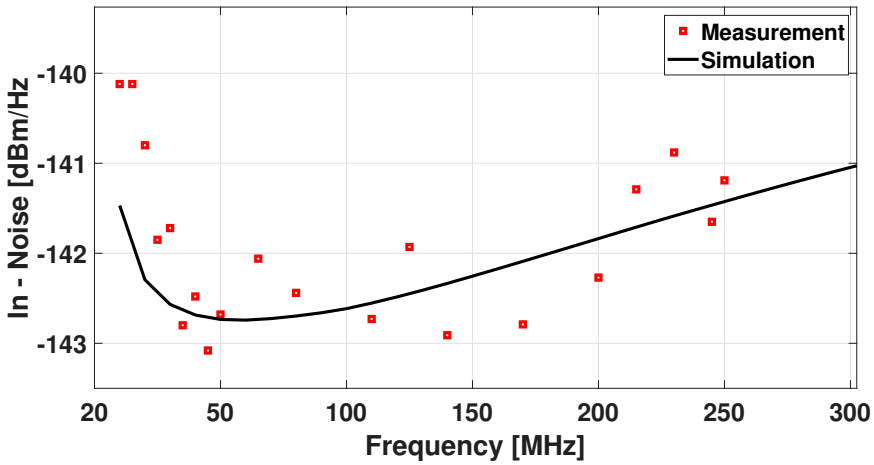

Figure 2.21: Input referred noise (up to $500MHz$).

results in higher input impedance causing distortion to become dominant at higher frequency. Since typically the first term dominates In-band (IB) and at out-of-band (OOB) the second term start to dominate. However, this may not be true when the bandwidth is extremely high and a significant capacitance loads the output, as shown in figure 2.20a. This indicates that, because of the last stage low gain, the distortion brought on by transconductance predominates also IB, and that IIP3 drops with frequency since the last stage must absorb both the input current and the current required by the load capacitance. This is supported by the simulation with C_L set to $250fF$ in figure 2.20a.
The simulated and measured IM3 vs. intermodulation tone position is shown in figure 2.20b. The decrease in loop gain, which begins at about $100MHz$ (Fig. 2.16), causes the IM3 to increase as it approaches the band edge.
The output noise density up to 500 MHz, with an integrated in band value (Vn) of $330\mu V$, is shown in figure 2.21. Due to Capacitor C_{IN} of figure 2.15, which causes the op-amp input referred noise to experience a gain to the output that grows with frequency, therefore, the output noise has a high pass shape.

Table 2.3 presents a summary of TIA performance and a comparison to the state-of-the-art. A figure of merit defined as $FoM = DR + 10log\left(\frac{NBW}{P_{diss}}\right)$ is used. Where DR stands for dynamic range defined as

$\left(\frac{2}{3}\right)(OIP3[dBm] - V_n[dBm])$, OIP3 is the output IP3, V_n is the integrated output noise, N is the filter order, BW is the bandwidth expressed in Hz, and P_{diss} is the power in watts.
Even with a 3 times higher bandwidth, this filter's FoM is $10dBJ^{-1}$ better than [23] and $4dBJ^{-1}$ better than [24]. On the other hand, even though this filter is just first order and [24] is a third order filter, the area with regard to [24] is 1.5 times larger. The inductors make up the majority of this filter's area, which can be decreased as the UGBW is increased, as was already mentioned.

	[23]	[25]	[24]	[26]	This Work
Technology [nm]	180	180	28	65	28
Area [mm^2]	N/A	1	0.04	0.037	0.06
Supply [V]	1.8	1.5	1	1.8	1.5
Power diss. [mW]	90	175	5.6	14.2	17
BW_{-3dB} [MHz]	500	1000	459	80	500 - 1500
Fiter Order	5	4	3	2	1
OP-1dB [dBm]	N/A	N/A	4.9	N/A	10
IB-OIP3 [dBm]	26.5	17.5	12.1	33.4	33
$V_{\mu V_{rms}}$	402	N/A	120	248.5	300
IMFDR3 IB [dB]	55	N/A	53.5	61.7	60.2
FoM [dBJ^{-1}]	159.4	N/A	165.7	162.2	169.7

Table 2.3: The comparison with the State-of-The-Art.

Chapter 3

Full Receiver Architecture

Abstract
The selection of a wireless receiver is an important phase in the receiver design since 5G has different requirements for wireless receivers than earlier standards did. The current-mode direct conversion receiver for the 5G mm standard will be presented in this chapter.

3.1 Proposed Receiver

For a 5G mm-wave transceiver, a current-mode direct-conversion receiver is designed using 28nm CMOS technology. Figure 3.1 shows the receiver block

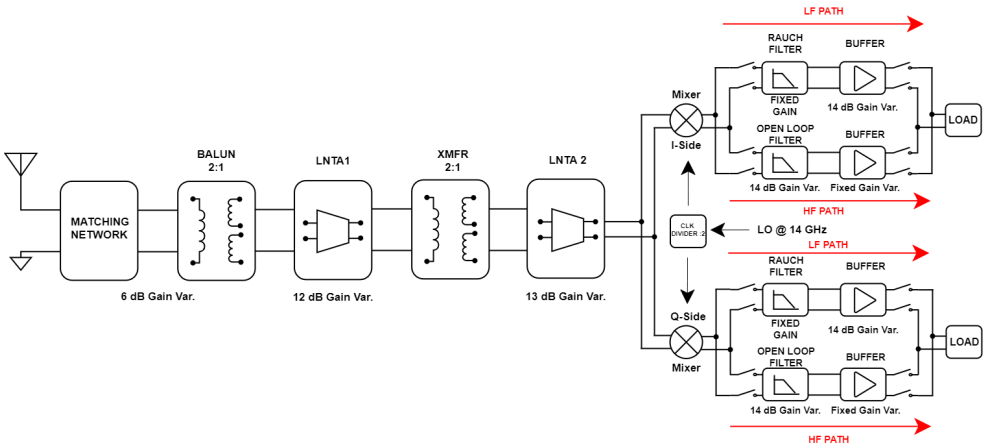

Figure 3.1: The block diagram of the implemented receiver.

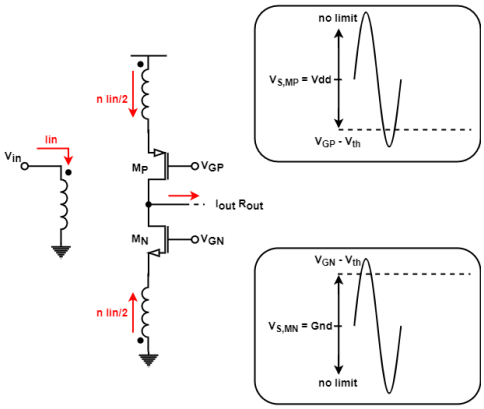

Figure 3.2: Simplified single-ended schematic of CG LNTA.

diagram. The RF signal from 7 GHz is down-converted to the baseband. There are two paths in baseband; one is called low frequency path and has an RF channel bandwidth of 50MHz to 400MHz, while the other is called high frequency path and has an RF channel bandwidth of 800MHz to 2GHz. Switches that are digitally controlled are used to control the baseband path selection.

3.2 Front-End

The front-end design is described in summary below, with more detail available in [27].
Two cascaded transconductance LNAs compose the front-end (LNTA). Trifilar transform, which also functions as a balun for matching, is used to biased the first LNTA. Similar to this, the second LNTA is biased using a trifilar transformer. Both trifiliar transformers have a 2:1 turn ratio and provide a 12dB current gain. Since it is challenging to achieve large gain at baseband because of the large bandwidth, these two LNTA are employed to provide it. The total transconductance gain with this configuration is 80mS under matching conditions. A whole receiver should have a gain variability of 45 dB, whereas the front-end have a variability of 31 dB (see Fig.3.1).

The circuit is designed around a trifiliar transformer. The signal is fed to the two inputs of LNTA through two identical secondary coils. Transformers are used to provide class AB behavior and low noise biasing by allowing the source voltage of the input transistors to move above supply and below ground,

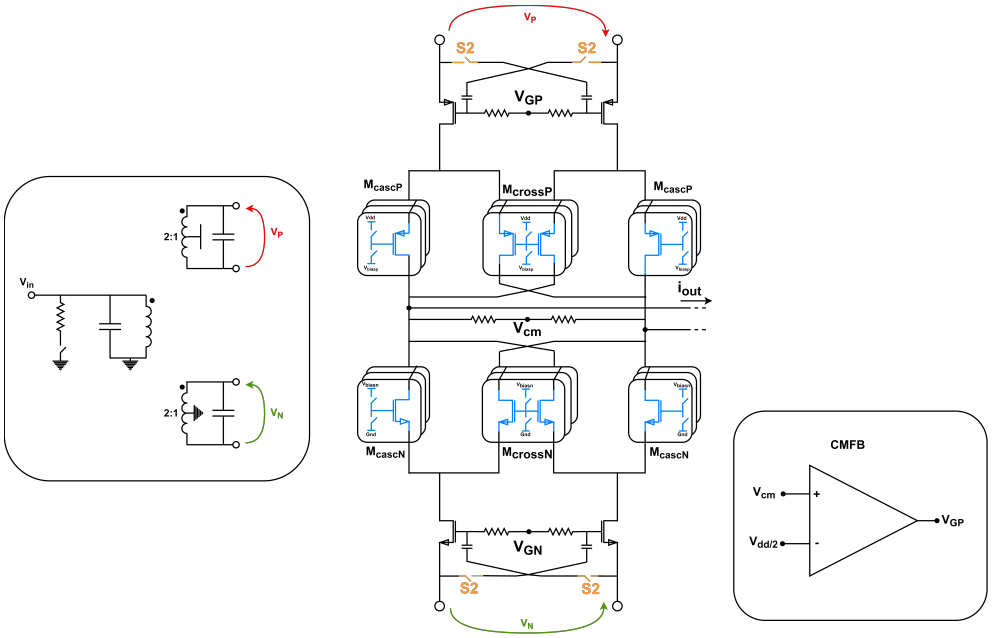

Figure 3.3: The complete schematic of first LNTA.

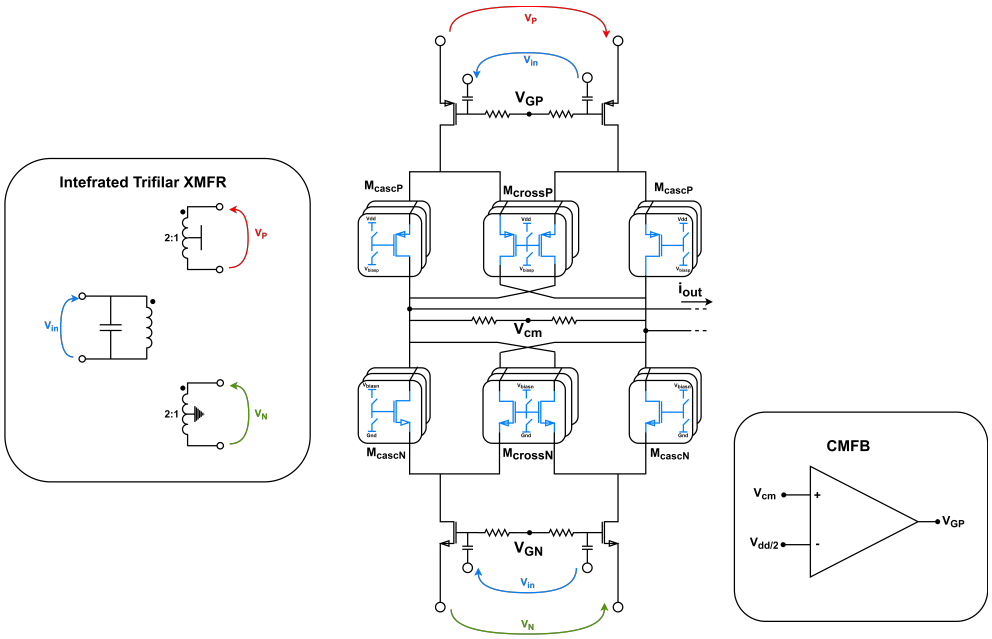

Figure 3.4: The complete schematic of second LNTA.

as shown in figure 3.2 [28]. Furthermore, the turn ratio n:1 (where $n \geq 1$) between the primary and secondary lowers the voltage swing and provides the current gain at the secondary. Reducing swing at the source of the input transistors improves linearity, achieving current gain at no linearity penalty. Ideally, input cannot be compressed, but output can if the load impedance is high. The low output impedance, however, implied by the current-mode operation leads to excellent linearity and compression point. In traditional CG amplifier's, the NF is given by:

$$NF_{CG}(s) = 1 + \frac{\gamma}{gmR_S}, \tag{3.1}$$

where γ is the MOS excess noise factor, R_s and gm are source resistance and MOS-transconductance respectively. Cross-coupling capacitors are used to cross-couple the input transistors' gates in order to reduce noise. These capacitors double the vgs voltage by applying an opposite-sign copy of the input signal from the source input transistors to the gate. The transistors' gm is increased by a factor of 2 in this technique, improving noise performance without using any extra power. Therefore, in matching condition NF becomes as follow:

$$NF_{CG}(s) = 1 + \frac{\gamma}{4}. \tag{3.2}$$

Since the transformer is attached to the input pins and adds its noise directly to the source noise, lowering the NF, the transformer's design is crucial. The transformer should have a coupling coefficient close to one and a high Q to minimize losses and reduce intrinsic noise. This led to the thickest metal layer (Metal 8 and alluminum metal (AP)) being used in the design of the transformer. With a turn ratio of 2:1, the transformer has been constructed using stacked topology and the thickest metal layer technically available in technology (Metal 8 and aluminium metal (AP)).
Current-steering approach is used to perform the gain variation in LNTA. Figure 3.3 shows the LNTA's entire schematic. The current is steered from one branch to the other as a result of the cross-coupling between the transistors McrossP and McrossN, which reduces the current gain.
Figure 3.4 shows the second LNTA's full schematic. It has the identical design as the first LNTA. However, in this situation, the passive boosting technique is used by connecting the input transistors' gates to the primary side of the transformer rather than cross-coupling the capacitors. As a result, the input transistors' gm is increased by a facto $1 + n$ in comparison to the CG stage, where n is the transformer's turn-ratio (n:1).

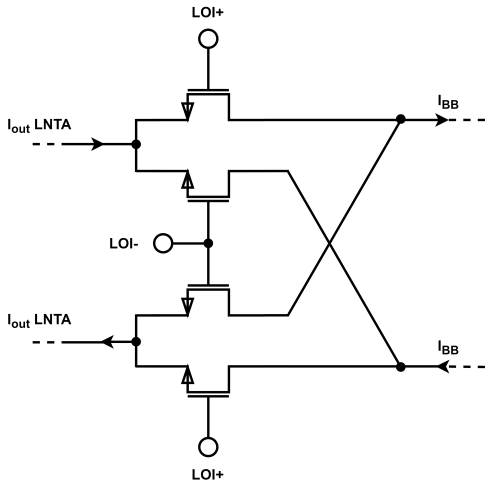

Figure 3.5: The schematic of mixer (I-side).

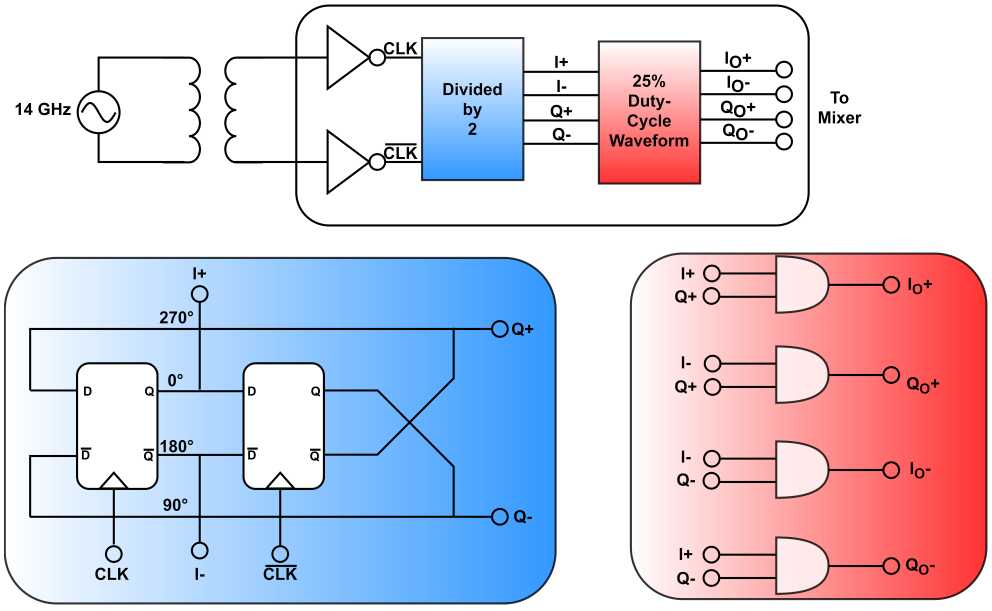

Figure 3.6: 251% duty-cycle Divider.

The RF signal is down-converted using a current-mode passive mixer. Figure 3.5 illustrates how both I and Q paths have double balanced mixers to handle differential input current. Waveforms with a 25% duty-cycle of LO are used to drive the mixer's switches. Due to the finite rise and fall times, the 25% duty-cycle option avoids the problem of overlapping, therefore related branches are never ON at the same time.
Through a 25% duty-cycle divider, whose schematic is shown in figure 3.6, the mixer's LO waveform is generated.

3.3 High Frequency Baseband Path

As previously stated, the baseband contains two paths, one known as the HF-path and the other as the LF-path. The HF-path is made up of an open-loop current mode filter followed by a wideband TIA, which covers an RF bandwidth of 800MHz to 2GHz. Even though closed-loop TIA was used in traditional BB architecture, this method becomes unworkable as channel bandwidth increases. The cause is that a large shunted capacitor must be connected to virtual ground in order to provide low input impedance and improve linearity, however as discussed in chapter 2, this method degrade noise since it exhibits a high pass transfer function for the input noise of OTA.

3.3.1 Open-Loop Filter

A Common-Gate (CG) stage, whose architecture is depicted in figure 3.7a, can be used to build an open-loop filter that promises to have a wide bandwidth. Rs represents the driving impedance provided by the LNTA and Mixer. By taking a closer look at the circuit, the frequency behavior of the input impedance may be roughly defined. Input impedance is determined by $1/gm$ at low frequencies; as the frequency increases, the capacitor C shunts the vgs; and if R is greater than 1/gm, an inductive behaviour is guaranteed. The circuit resembles an RLC network when the capacitor C_{in} is connected in parallel with the impedance Z_{in}. As a result, the current passing through is a result of a second-order low-pass filter on the input current.
There are two significant drawbacks. The first is that in order to increase the gm of the CG to lower the input impedance, a significant current is needed. Since the limited voltage supply necessitates a lower resistance R_L, which increases its noise contribution, this could be a concern from a noise perspective. The second problem that Q is proportional to the R_S, which is problematic because the mixer's equivalent driving impedance tends to decrease as the LO frequency increases. This can be explained intuitively by remembering that

R_S appeared parallel with the equivalent inductor provided by the CG.
Using regulated cascode design, which connects an amplifier A to the source and gate of the CG stage, the first problem may be solved. As seen in figure 3.7b, this approach reduces the input impedance by a factor of 1+A. As a result, with this technique, for the same current, a lower input impedance compared to the CG filter can be obtained. With this method, R_L noise contribution is reduced by a factor of $1 + A$.
Cross-coupled transistors with diode connections make up the amplifier A, which has a gain of -1. The resistor R is given by $1/gmd$, where gmd is the transconductance of the diode-connected mosfet. The noise contribution of gmd limits its lower value, whereas power consumption limits its upper value. gmd value is chosen so that it continues to contribute less noise than CG's noise contribution. Although the noise problem is resolved with this solution, the Q is still limited by R_S. At the input of the CG amplifier, a negative capacitance using the miller effect is applied to address this problem. Figure 3.8 shows the complete circuit with the negative capacitor, and in [29] more

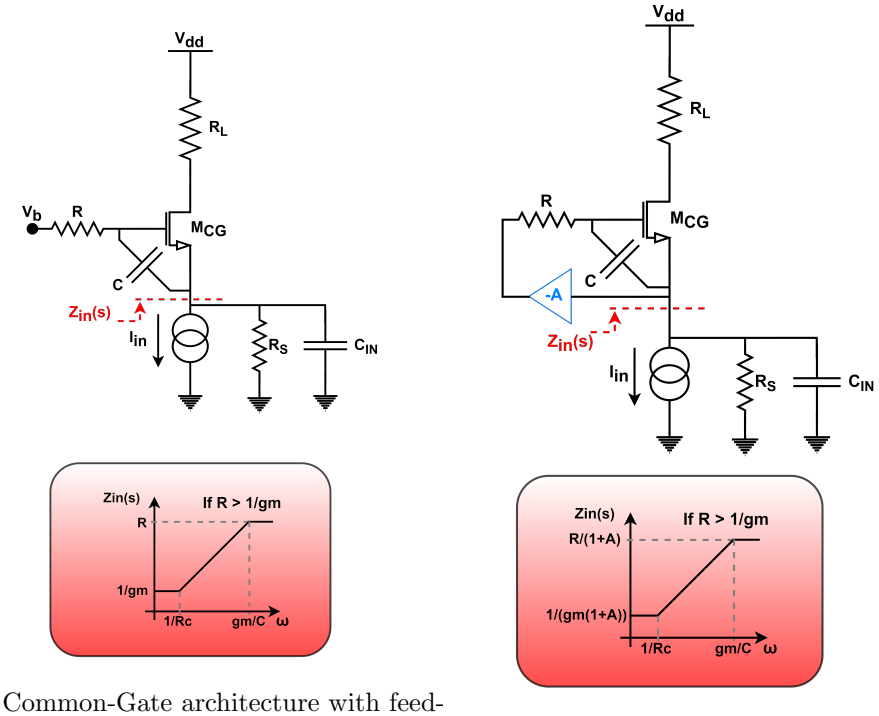

(a) Common-Gate architecture with feed-forward capacitor C.

(b) Regulated cascode architecture.

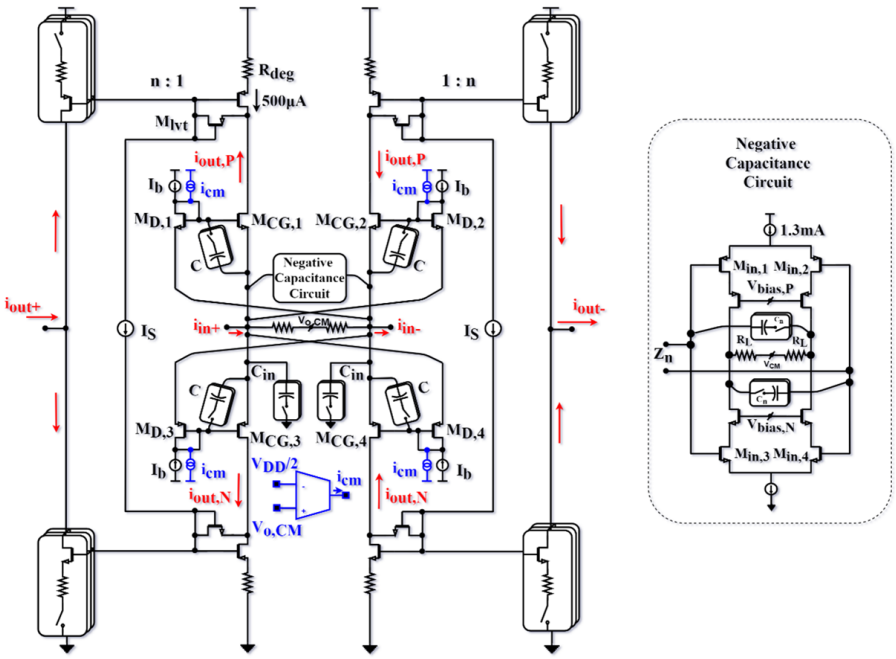

Figure 3.8: The complete schematic of open-loop filter with negative capacitance.

information is available.

3.3.2 Wideband TIA

The TIA that is used in full receiver has been modified from the one that is presented in chapter 2 (Fig.3.9). In particular, the inductor has been removed to save space and power. The overall performance of the TIA will negatively impact of these modifications.
The identical circuits that was used for the TIA in chapter 2 is also being used to implement the OTA, except for a few adjustments to the bias current and time constant. One significant distinction is that, unlike other design, this one uses capacitive boosting solely by the FF stage rather than also by the second stage. This is done in order to stabilize the circuit by giving the FF stage extra gain, as shown in figure 3.10.
As can be seen from Table 3.1, the OTA transconductance is much lower than that of the prior design. The performance will suffer as a result. Figure 3.11 illustrates how the TIA's loop gain has decreased, particularly UGBW from

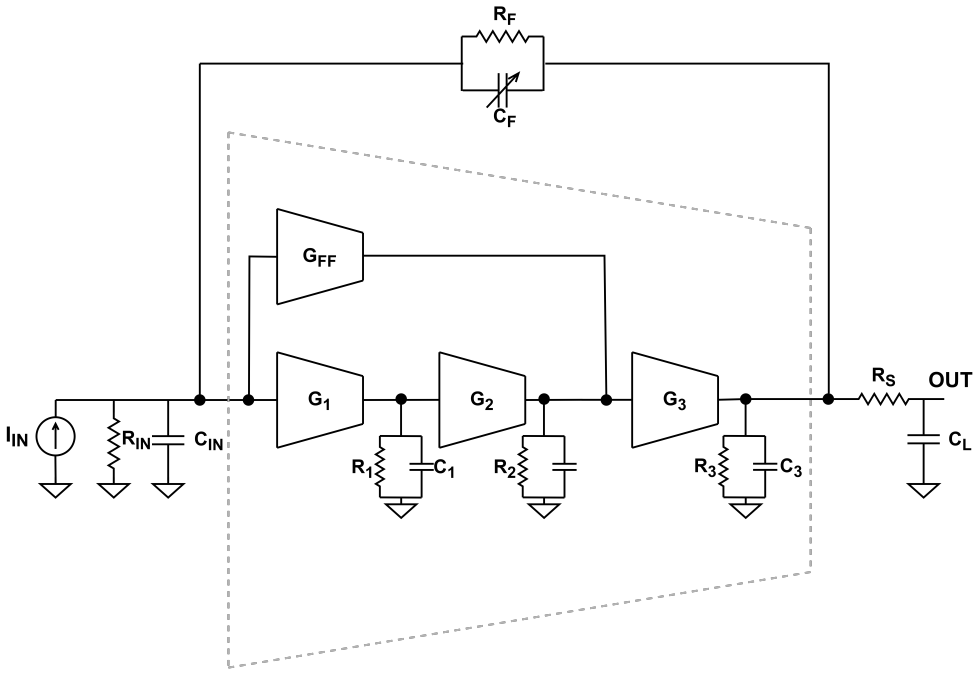

Figure 3.9: The block diagram of the implemented TIA.

7.5GHz to 4.3GHz, and how the loop gain at 1GHz has decreased from 27dB to 15.8dB. One thing to consider is that the FF stage's transconductance is significantly higher than the main path's. This supports the preceding chapter's explanation that a significantly larger transconductance must be employed on the FF stage in the absence of inductor-based stability. The comparison between the high power (chapter 2) and low power TIAs is shown in the table 3.2. The power is nearly cut in half, and the area is reduced by 7.5 times. Because loop gain has been decreased, distortion performance has also been decreased. In fact, the IB-OIP3 is lowered from 30 dBm to roughly 20 dBm. The 1-dB compression point is 6.7 dBm as a result of the last stage's reduced gain.

3.4 Low Frequency BaseBand Path

As shown by figure 3.1, the LF-path is a third order baseband filter that is made up of a second order Rauch filter and a first order TIA, covering a range of RF channel bandwidths from 50MHz to 400MHz.

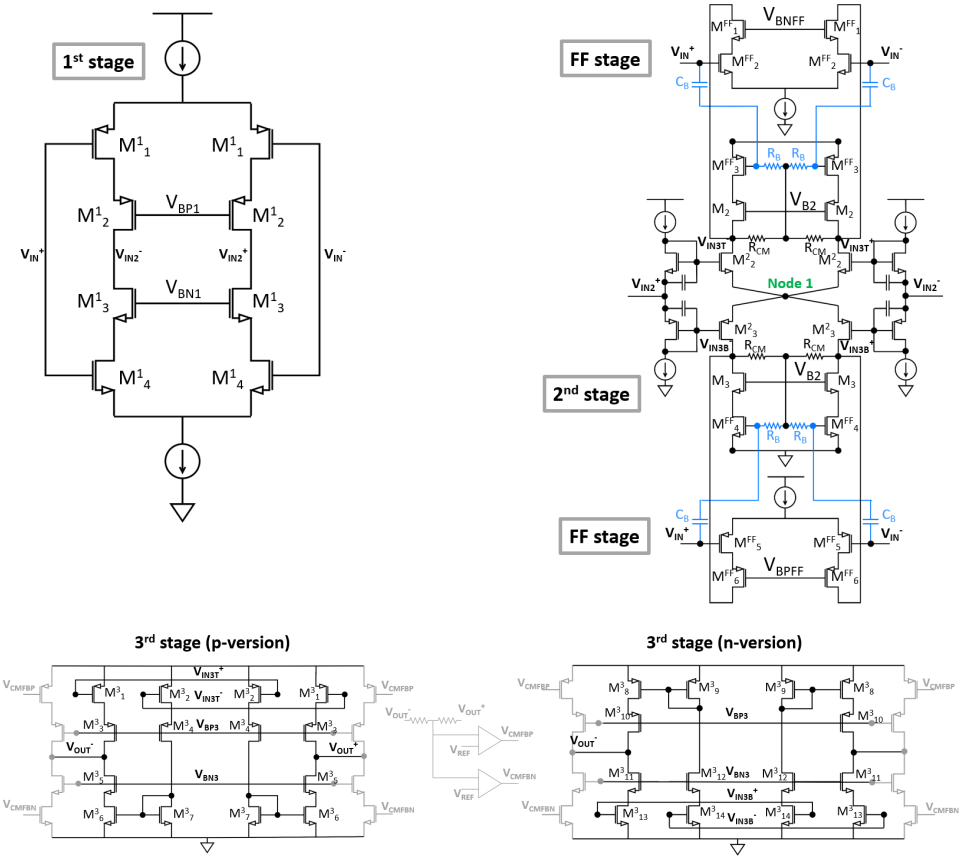

Figure 3.10: The Complete Schematic of OTA.

Stage	Gm
1_{st}	$3.2mS$
2_{nd}	$3mS$
FF	$21.85mS$
3_{rd}	$12.31mS$

Table 3.1: The design parameter of the implemented TIA

The rauch filter was designed using an FF design approach, with four stages in the main path and FF starting from the output of the first stage to

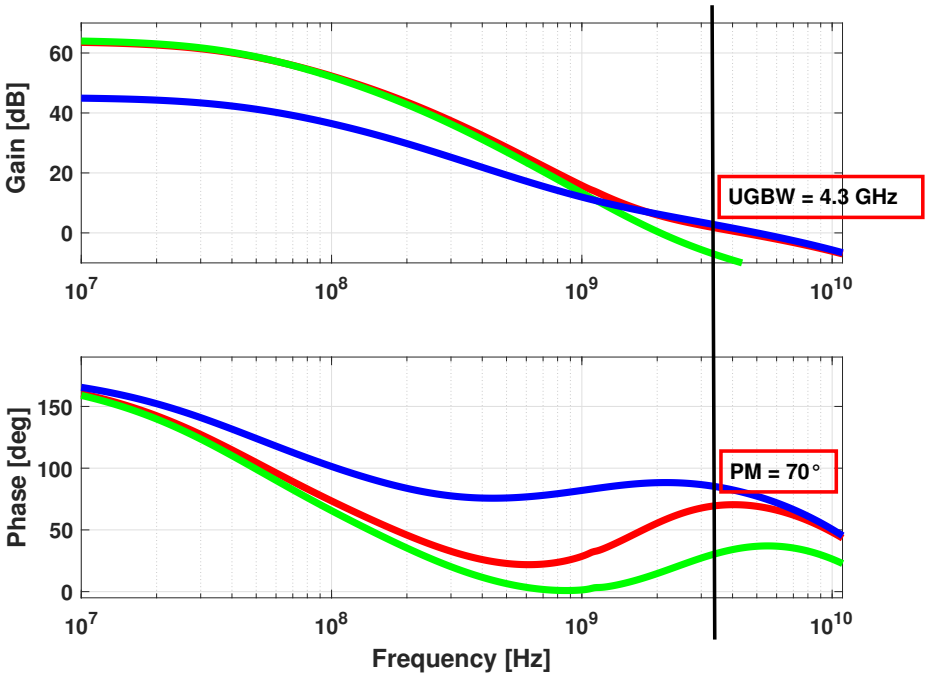

Figure 3.11: The Loop Gain of the TIA.

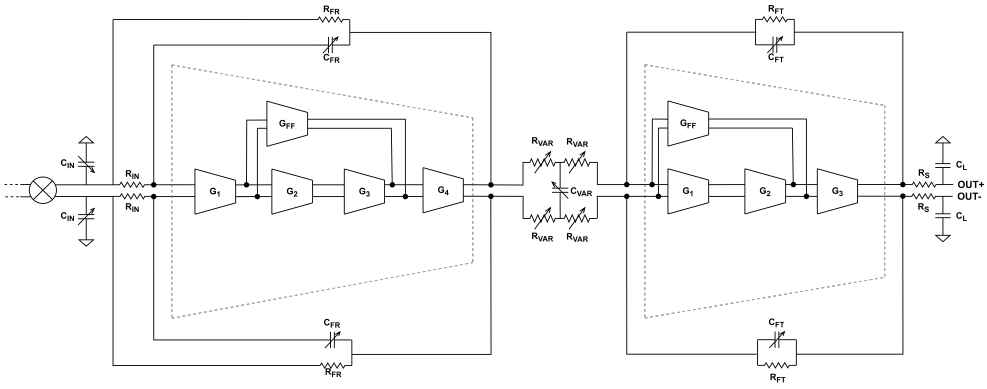

Figure 3.12: The block diagram of low frequency baseband path.

	H-Power	L-Power
Technology $[nm]$	28	28
Area $[mm^2]$	0.06	0.008
Supply $[V]$	1.5	1.5
Power diss. $[mw]$	17	8
UGBW $[GHz]$	7.5	3
LGain @1$GHz[dB]$	27	14.7
BW$_{-3dB}$ $[MHz]$	500 - 1500	500 - 1500
OP$-1dB$ @1$GHz[dBm]$	10	6.7
IB$-OIP3[dBm]$ $f_{IM3} = 700MHz; f1 = 800MHz; f2 = 900MHz$	30.2	19.84

Table 3.2: High Power and Low Power Comparison

the output of the last stage. As a result of this strategy, stability is assured with a 68° phase margin and 2.4GHz UGBW. Since the FF path exhibits a positive loop for common mode signals, special attention must be paid to the common mode response. As a result, the common mode loop gain of the FF path must be below zero to ensure the stability of common mode signals. With a peak at 10GHz of -40dB, this design achieves a good common mode response. Refer to [30] for more information about the rauch design.

The same TIA that is utilized in HF-path implementation also used to LF-path. The TIA's bandwidth can be programmed, and the C_{FT} capacitor can be varied to change it. Additionally, the gain can be programmed by modifying the resistor R_{VAR}.

To increase attenuation, an extra pole is provided at OOB using the capacitor C_{VAR}. When both the bandwidth and the gain are changed, this capacitor should also be changed in order to move the OOB pole and achieve the desired attenuation.

Chapter 4

Measurement Results of Full Receiver

Abstract
The measurements for the full receiver reported in the previous chapters are presented in this chapter. The measurement setup will be explained first, followed by experimental results for both the high-frequency and low-frequency paths. It will be discussed how effectively the receiver performs in terms of input matching, transfer function, linearity, and noise. At the conclusion, a table containing the obtained measurement results and the target requirements will be given.

4.1 Full Receiver Experimental Results

TSMC 28nm HPC technology is used to implement the receiver. The receiver's layout and a microphotograph of the chip are shown in Figure 4.1. Chip dimensions are $1.4mm \times 1.4mm$, and the active area is $0.763mm^2$. The chip is mounted on a PCB, the power supply and biasing pads are wire bonded, and the input and LO signals are applied directly to the pads using single-ended and differential probes, respectively. For testing reasons, two PCB boards have been created; figure 4.2 depicts the measurement setup. The biasing and digital bits are provided by one board, and the chip on the probe station is tested by another. The *Cascade Infinity GSG* single-ended probe is used to provide the input signal to the chip from the *Agilent E8257* signal generator. The *cascade infinity GSGSG* differential probe connects to the *Anritsu MG3693A* signal generator to provide the differential LO signal. A *R&S RT-ZD40* probe is used to sense the outputs, and an *R&S FSQ8* signal analyzer is used to measure

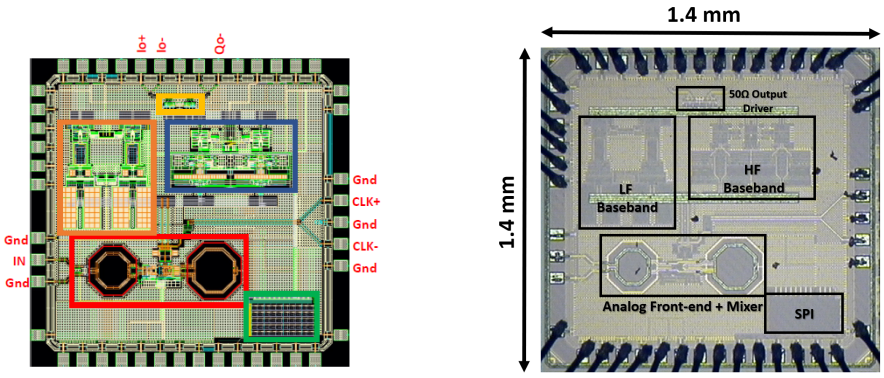

(a) (b)

Figure 4.1: (a) The layout of the full receiver. (b) The microphotograph of the chip.

them. Digital bits are generated using an *NI-USB8451 SPI* interface, while biasing currents and voltages are applied through an *NI cRIO-9014* using Labview software.

4.1.1 Measurement Results: High Frequency path

As previously mentioned, the HF-path consists of a wideband TIA preceded by an open-loop filter. It covers BB bandwidth between 400MHz to 1GHz.

The S11 is shown in Figure 4.3 for both the highest (45dB) and lowest(0dB) receiver gain. The *Agilent E8361C PNA* network analyzer was used to do these. In both situations, a notch is visible around the carrier frequency (i.e., 7GHz), with S11 greater than -20dB for maximum receiver gain and greater than -35dB for minimum receiver gain. As can be seen, both cases demonstrate good matching conditions. Additionally, there is good matching for the target frequency (6 GHz to 8 GHz), with S11 better than $-12dB$ for maximum gain and better than $-15dB$ for minimum gain.

4.1.1.1 Receiver Gain

Using a signal generator with a frequency swept from 3GHz to 11GHz, receiver gain was measured. The gain versus frequency for the upper and lower band at the 7GHz LO frequency is shown in Figure 4.4. The in-band gain is 45dB, which fulfills the specifications. For the lower band and higher band,

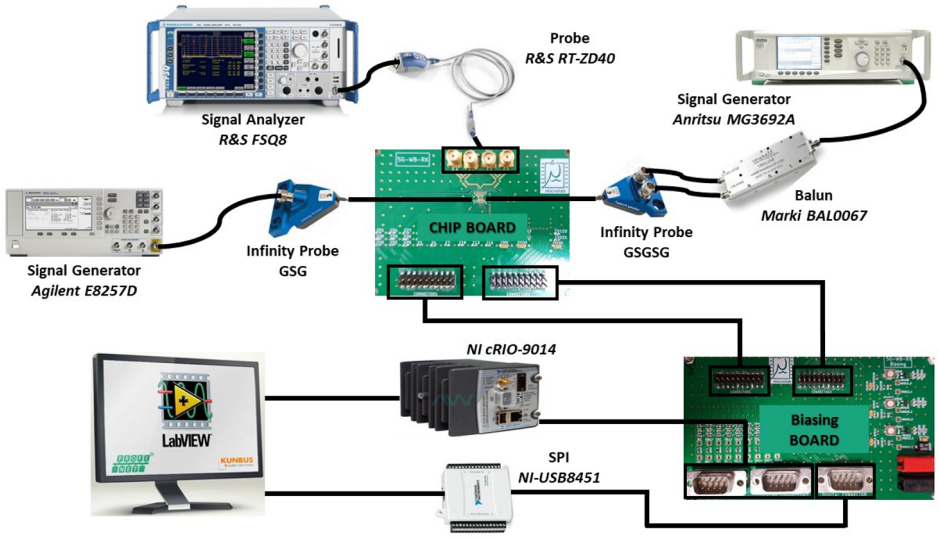

Figure 4.2: The measurement setup for characterization of the receiver.

the down-converted gain at the band edge (i.e. 1 GHz) is only reduced by 1.6dB and 2.3dB, respectively. The OOB selectivity from 1GHz to 4GHz is 50dB, which is significantly higher than the specification of 33dB. This means that a comparable 4th-order filter is produced utilizing an open-loop filter and wideband TIA. Around 1GHz, there is a mismatch between the upper and lower bands of less than 1dB.
The gain is adjustable between 45dB and 0dB. (Fig.4.5). The open-loop filter achieves a 14dB gain fluctuation in the baseband, which is done in 4 steps

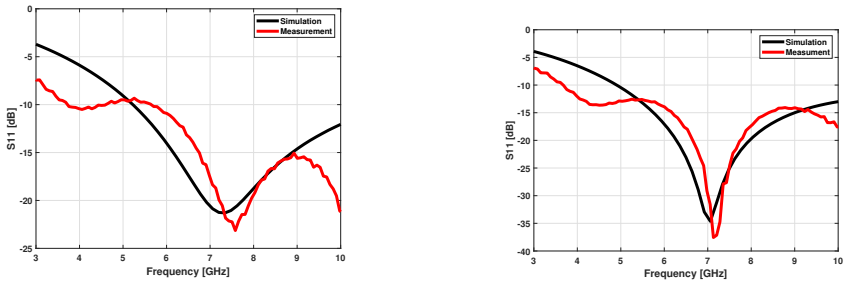

(a) **(b)**

Figure 4.3: Measurements of S11: (a) for max Rx gain (b) for min Rx gain.

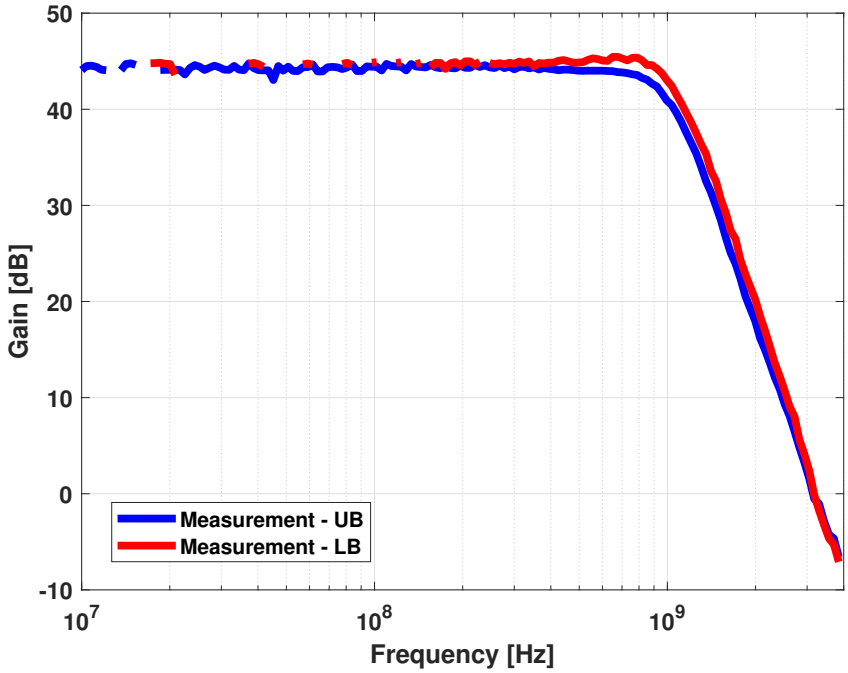

Figure 4.4: The down-converted receiver gain for lower and upper band.

with the help of digital bits from the SPI interface. The bits in the open-loop filter regulate the current-mirror branches, which alter the current gain. The last 31dB is achieved in the front-end using the current steering technique in two cascaded LNTA (25dB of gain variation), as well as passive attenuation in front of the balun (6dB of gain variation)
Figure 4.6 illustrates the bandwidth variation (from 400MHz to 1GHz) that is made possible by using digital bits to control the capacitors in wideband TIA and open-loop filters. The measured OOB selectivity from band edge to 4x-band edge is higher than 33dB throughout the entire channel bandwidth, which satisfies the requirements.

4.1.1.2 Linearity and Compression Measurements

Using a Suhner-4901 power combiner, a two-tone test that combined signals from Agilent E8257 signal generators was used to measure the receiver's linearity. Two tones were injected at 400MHz and 500MHz, causing the IM3 to fall at 300MHz (at BB frequency). In-band IIP3 yields -18.93dBm for the

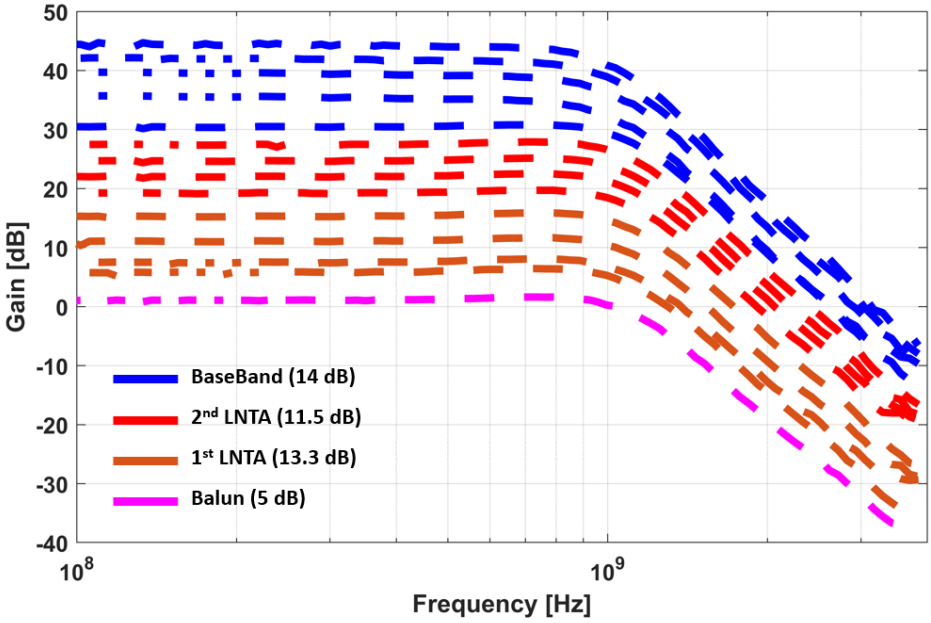

Figure 4.5: The measured receiver gain variation for the HF-BB path.

maximum receiver gain (45dB). Figure 4.7 shows the OIP3 in relation to the variation in receiver gain for the two tones at 400MHz and 500MHz, and the IM3 at 300MHz. OIP3 is greater than 25dBm for all configurations, meeting the requirements (15dBm).

Additionally, the receiver's compression was tested for both the maximum and minimum receiver gains. The in-band compression for the maximum receiver gain, as illustrated in Figure 4.8a, was carried out using a tone at $f_{LO}+300MHz$ and sweeping the input signal's power, yielding an In-P1dB of $-27.5dBm$. The same procedure was carried out with a tone at $f_{LO}+700MHz$, yielding an In-P1dB of $-33dBm$. The input referred in-band 1dB compression for the minimum receiver gain, which yields $+9dBm$, is shown in Figure 4.8b with a tone at $f_{LO}+700MHz$. The receiver satisfies the specifications of $+6dBm$ for minimum receiver gain and $-39dBm$ for maximum receiver gain of 1dB compression point.

4.1.1.3 Noise Performance

Figure 4.9a depicts the NF in the scenario with the maximum receiver gain (45dB) and maximum bandwidth (1GHz). In the post layout simulation, an

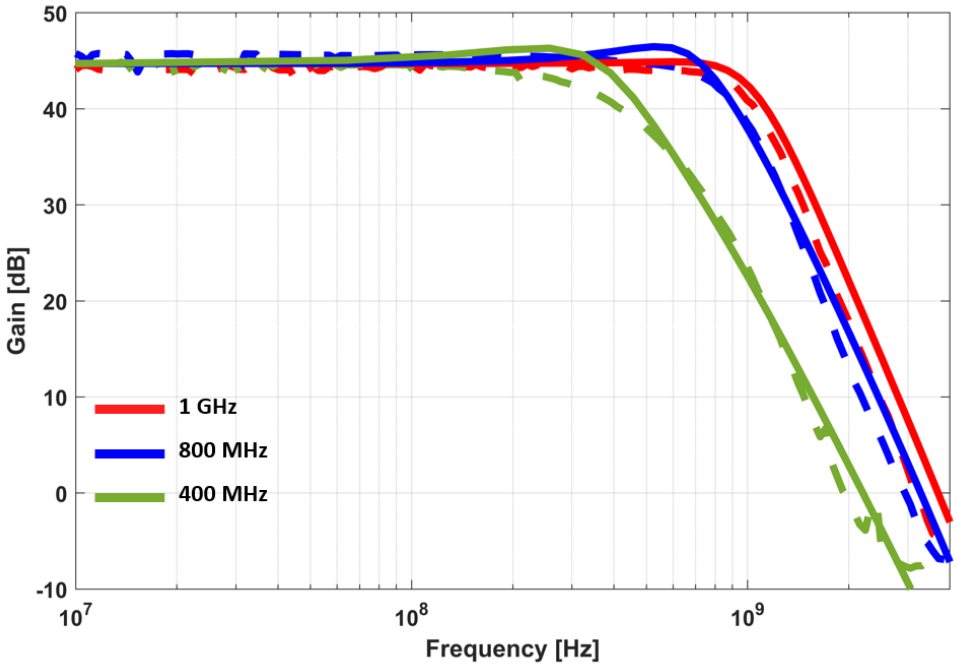

Figure 4.6: The measured receiver bandwidth variation for HF-BB path by changing the BW of second order open loop filter and TIA.

integrated NFdsb of 5.6dB is attained within the bandwidth of 1GHz. Due to its high noise floor, the wide bandwidth probe (R&S RT-ZD40) used to test receiver gain has an inbuilt attenuation of 20dB that limits noise measurements. LeCroy AP033, a low frequency probe with a 500MHz bandwidth, was employed. Noise measurements are therefore restricted to 500MHz, giving an integrated NFdsb of 5.75dB. Figure 4.9b displays the integrated noise contribution at the output of block that composed the receiver. Over a 1GHz bandwidth, the total integrated output noise is 2.8×10^{-15} V^2rms. Due to the front-end high RF gain, the front-end makes up about 48% of the output noise while the baseband makes up 15%. The majority of the noise for the front-end part comes from the first LNTA and the balun, whereas the majority of the noise for the baseband section comes from the open-loop filter. Figure 4.10 displays the integrated NFdsb with respect to receiver gain. For a 45dB maximum receiver gain, the NFdsb is 5.6dB. As the receiver gain decreases, the NF starts to rise. The receiver gain begins to decline from the baseband. After 14dB of attenuation, the NF only increases by 1dB, giving

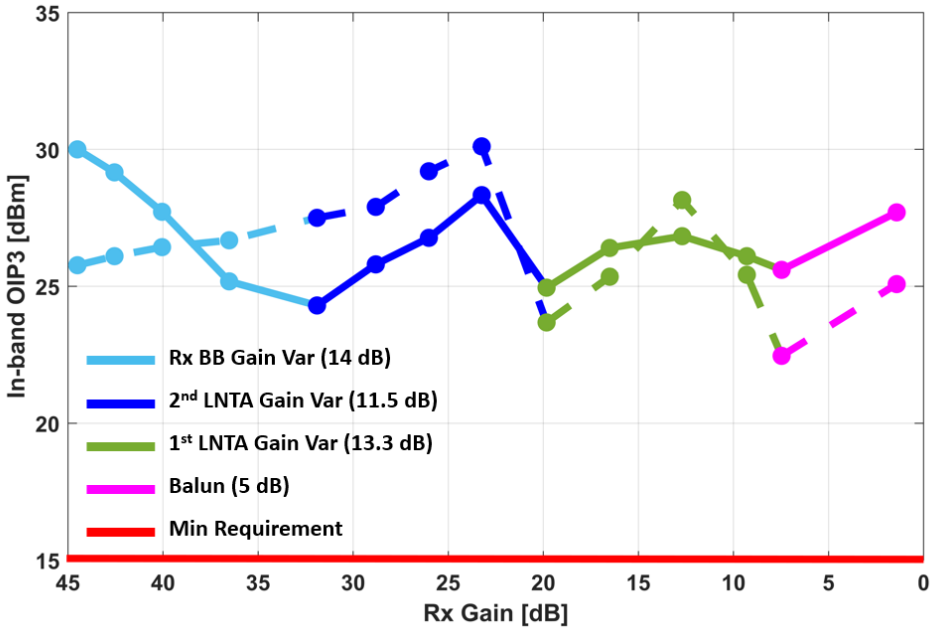

Figure 4.7: The in-band OIP3 vs. receiver gain. The results are obtained by adding two tones at f_{LO}+400MHz and f_{LO}+500MHz so that the IM3 falls at 300MHz.

ample room to meet the requirement of 0.7dB of noise figure increase for every dB of gain loss. The contribution of the cascode and cross-coupled transistors became dominant after 25dB of attenuation in the two cascaded LNTA, and the NF climbed up to 27.5dB from 6.5dB. The matching network's last 6dB of attenuation increases the NF by 5dB. The measurements and post-layout results are in good agreement. For each dB of gain reduction, the NF slope remains below the minimal requirement of 0.7dB.

4.1.2 Measurement Results: Low Frequency path

Results of low frequency baseband measurements will be discussed in this section. It has a first-order TIA filter preceded by a second-order rauch filter, and its BB bandwidth ranges from 25MHz to 200MHz.

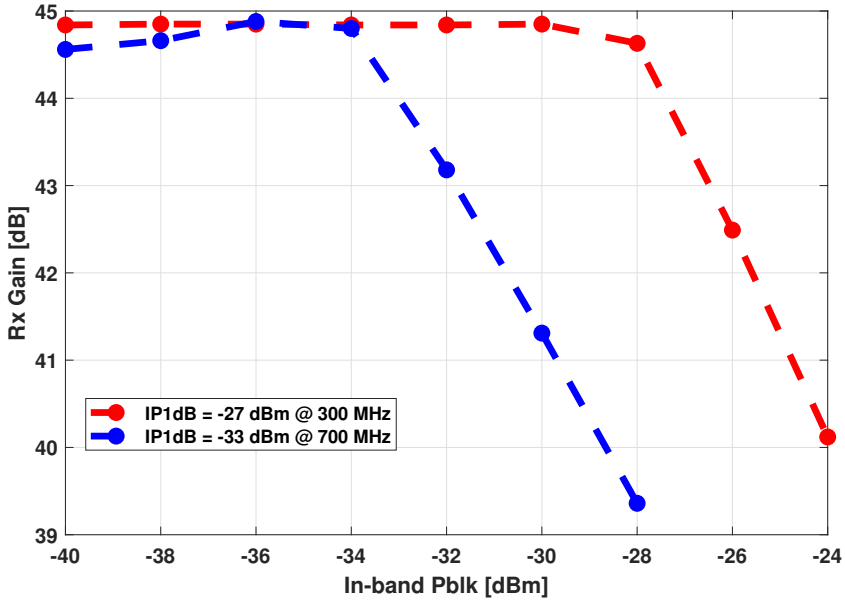

(a)

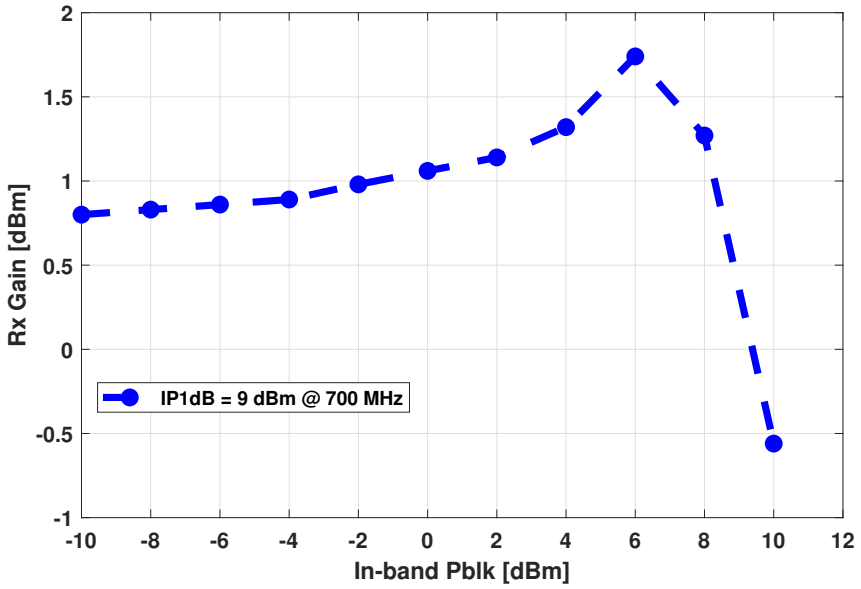

(b)

Figure 4.8: (a) the in-band compression for maximum receiver gain with blockers at $f_{blk} = f_{LO} + 700MHz$ and $f_{blk} = f_{LO} + 300MHz$ (b) the in-band compression for maximum receiver gain with blockers at $f_{blk} = f_{LO}+700MHz$.

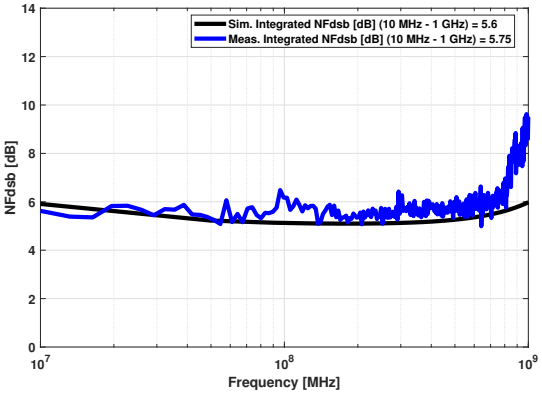

(a)

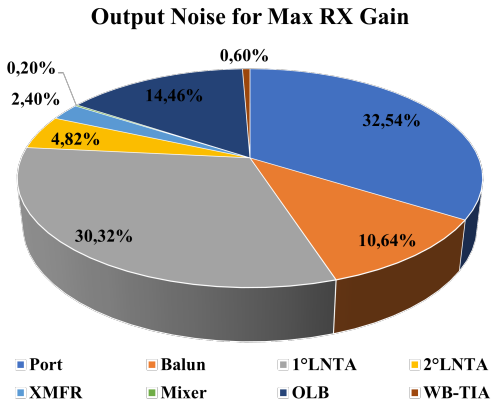

(b)

Figure 4.9: (a) NFdsb max Rx gain (b) output noise contribution for maximum Rx gain.

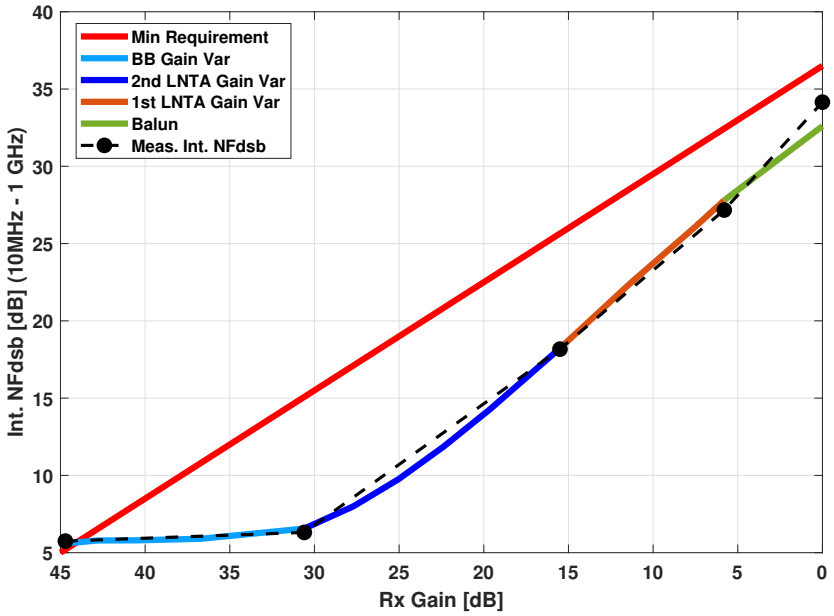

Figure 4.10: The NFdsb vs. receiver gain.

4.1.2.1 Receiver Gain

The receiver gain for the low frequency path is evaluated using the same test setup as for the high-frequency path. To measure the lower and upper bands of the receiver gain that are down-converted, a frequency sweep from 6.2GHz to 7.8GHz is generated at the input. The receiver gain, shown in Figure 4.11, is 45dB of in-band gain, and it is constant up to 200MHz. At the band edge, the difference between the lower and higher band is less than 2dB. It offers 34dB of OOB attenuation between 200MHz and 800MHz. The gain can be adjusted between 45dB and 0dB (Fig.4.12), same like in the HF path. The first-order TIA delivers the first 14dB of gain variation via a resistive divider. It is done by activating parallel resistors using switches that are controlled by digital bits. The front-end, just like for HF-path, provides the remaining 31dB of attenuation. OOB attenuation between band-edge and 4 x band-edge of more than +33dB is guaranteed for each configurability, as well as band-edge loss of less than 2dB.
The bandwidth variation between 25MHz and 200MHz is depicted in Figure 4.13. Both rauch and TIA vary the bandwidth; rauch does this by altering the

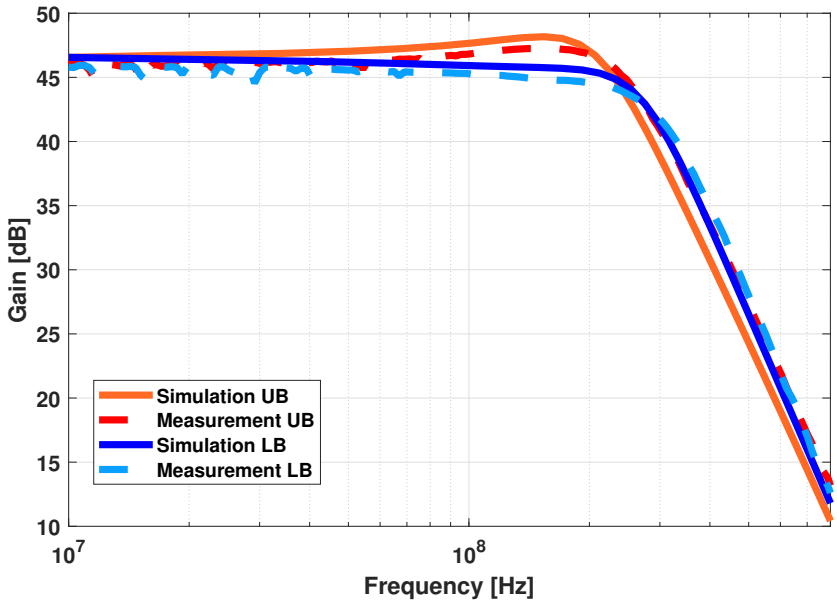

Figure 4.11: The down-converted receiver gain for lower and upper band.

feed-back capacitor and input capacitor of the rauch filter; TIA does this by adjusting the feed-back capacitor. Additionally, as for gain variability, OOB attenuation between the band-edge and 4 x band-edge of more than +33dB and band-edge loss of less than 2dB are assured.

4.1.2.2 Linearity and Compression Measurements

Similar to the HF-path, the two tone test was used to evaluate linearity. In order for IM3 to fall at 170MHz, two tones from f_{LO} at frequencies 175MHz and 180MHz were injected into the receiver. In the case of maximum receiver gain, in-band IIP3 is -23dBm. The OIP3 is depicted in figure 4.14 in relation to the variation in receiver gain, and it is clear that the OIP3 is above +21.4dBm for all gain configurations, well beyond the required +15dBm.

Compression measurements are carried out when the receiver gain is set to its maximum for a 200MHz BB-bandwidth. By injecting a tone at $f_{LO}+160MHz$, an in-band 1dB compression point was performed out, the tone's power was swept, and the output signal after downconversion was monitored. Figure 4.15 illustrates that the input 1dB compression point is -32 dBm, which satisfies the requirement of -39 dBm 1dB compression point for the receiver. Due to the

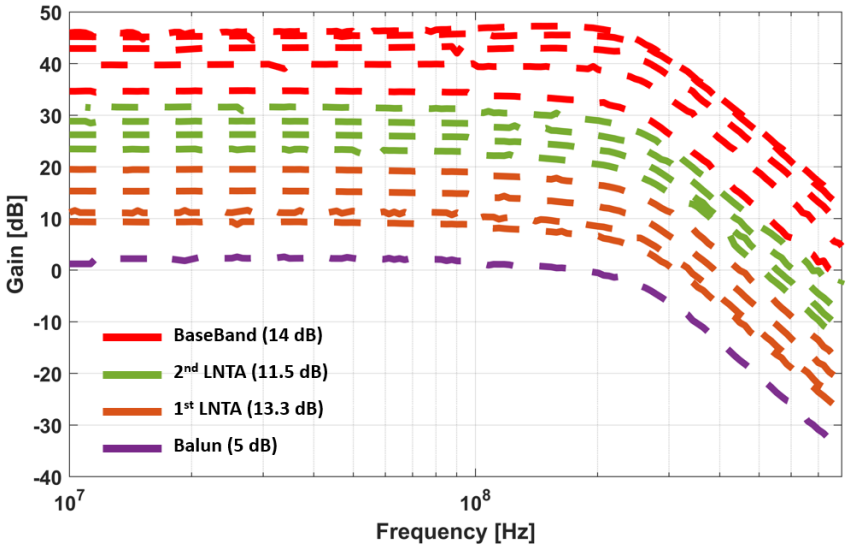

Figure 4.12: The measured receiver gain variation for the LF-BB path.

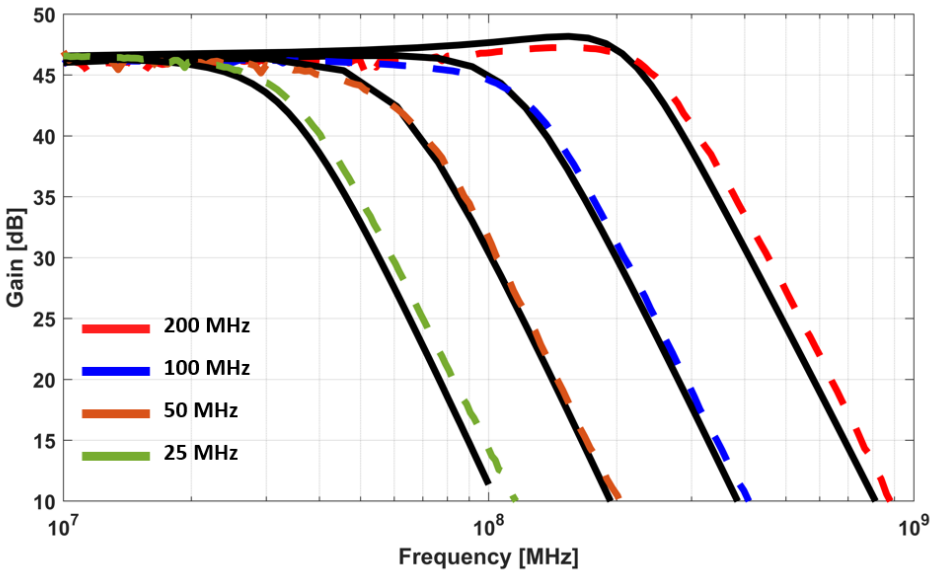

Figure 4.13: The measured (dashed-line) and simulated (solid-line) receiver bandwidth variation for LF-BB path by changing the BW of second order Rauch filter and TIA.

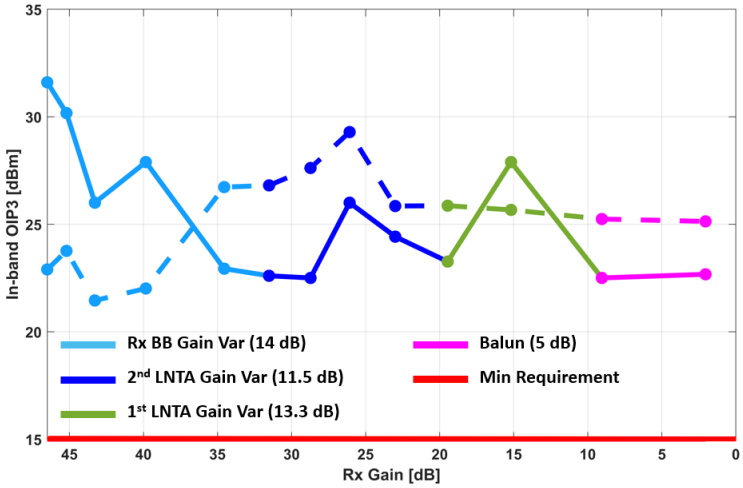

Figure 4.14: The In-band OIP3 vs. receiver gain.

signal generator's maximum output power (+10dBm), compression measurement is limited in cases of low receiver gain. The In-band 1dB compression point is therefore above +10dBm at minimum receiver gain, satisfying the +6dBm requirement.

4.1.2.3 Noise Performance

The NF is depicted in figure 4.16a under the conditions of maximum receiver gain and bandwidth. The Lecroy AP033 probe was used to measure noise. The obtained NFdsb of 5.82dB is almost identical to the post-layout NFdsb. Figure 4.16b depicts the receiver blocks' contribution to noise; the integrated total output noise from 10MHz to 200MHz is $7.63 \times 10^{-15}\ V_{rms}^2$. The majority of the noise, 49.1%, comes from the front end, with the balun and first LNTA contributing over 42%. The Rausch filter makes up the majority of the contribution in BB, 18.22%, whereas TIA makes just 0.22%. The NFdsb vs receiver gain is depicted in Figure 4.17. The NF grows as the gain decreases. The NFdsb increases from 5.82dB to 6.39dB when the BB gain decreases by 14dB. The NFdsb increases to 32.25dB as the receiver gain is reduced to its minimum value, and its slope remains below the minimal requirement of 0.7dB for each dB of gain reduction.

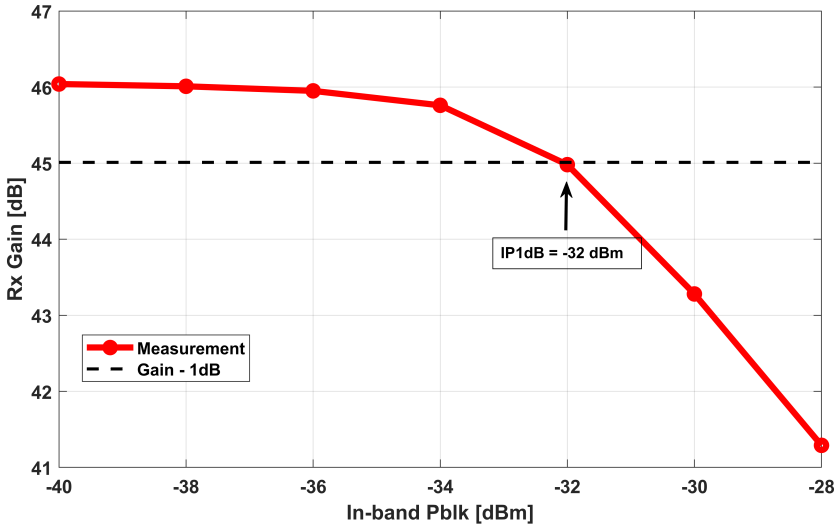

Figure 4.15: In-band compression for maximum receiver gain with blockers at $f_{blk} = f_{LO} + 160MHz$.

4.2 Receiver Performance Summary

Item	Condition	Specs	HF BB Path	LF BB Path	Unit
Carrier Frequency		7000	7000		MHz
RF Channel BW	Mode (50,100,400, 400, 800, 1600 and 2000)		400, 800 and 2000	50, 100, 200 and 400	MHz
Input VSWR	in all modes	1.5	1.32 (Max gain) 1.04 (Min gain)		
Gain Control Range	Max Gain	45	45		dB
	Min Gain	0	0		dB
Noise Figure	@LNA input, max gain	5	5.6	5.82	dB
Noise Figure Slope		0.7	<0.7	<0.7	dB/dB
Input P1dB	Max Gain, inband	-39	-33	-30.3	dBm
Input P1dB	Min Gain, inband	6	9	>10	dBm
OIP3	All gain step, $P_{RxOUT} = -8dBm$	>15	>23.5	>21.4	dBm
Analog Filter Selectivity	From Bandwidth to 4 x bandwdith	-33	>33	>33	dB
In-band Flatness	in all modes	1	2	0.5	dB
Power Consumption	Max gain, Max BW		68	51	mW

Table 4.1: Full receiver performance summary.

Table 4.1 shows measured receiver performance for both HF and LF paths. In the event of maximum receiver gain, the entire receiver satisfies all requirements with the exception of the NF. As previously stated, it supports RF

channels from 50MHz to 2GHz. The input VSWR is 1.32dB for the highest gain and 1.04dB for the lowest gain. Gain configuration options for the HF and LF paths range from 45dB to 0dB. The integrated noise figure for the LF-path is 5.82dB, with over 42% of the noise coming from the first-LNTA, which can be reduced by increasing its transconductance. While NF is 5.6dB in the case of the HF-path. For every dB gain reduction in both situations, the NF slop is below 0.7dB, meeting the requirements. The measured OIP3 is greater than 21.4dBm for the LF-path and greater than 23.5dBm for the HF-path for all gain steps, exceeding the required level. In the case of receiver compression, In-p1dB is -32dBm for LF-path with a blocker at 160MHz offset from fLO and -33dBm for HF-path at 700MHz offset from fLO for maximum receiver gain. Since the measurements are limited by the instrument, as previ-

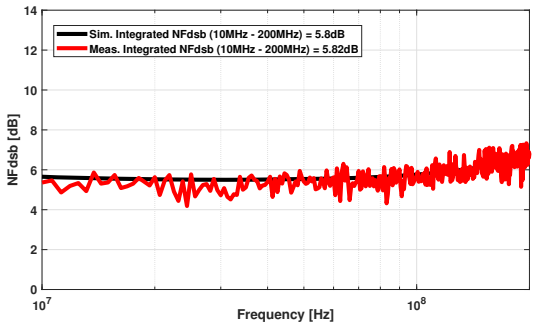

(a)

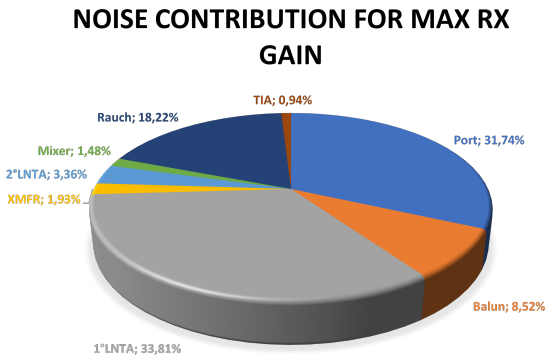

(b)

Figure 4.16: (a) NFdsb max Rx gain (b) output noise contribution for maximum Rx gain.

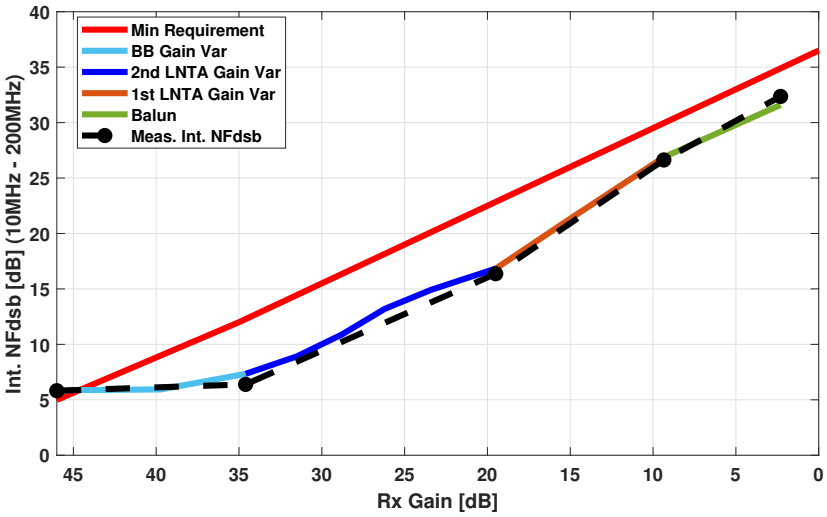

Figure 4.17: The NFdsb vs. receiver gain.

ously said, In-p1dB for the minimum receiver gain is over 10dBm for LF-path and 9dBm for HF-path. The measured selectivity for the LF and HF paths is well over 33dB for each gain and bandwidth configuration, and the in-band flatness is kept to less than 0.5dB for the LF path and less than 2dB for the HF path.

Figure 4.18 displays the power distribution of the full receiver for maximum receiver gain. According to figure 4.18a, the total power for the LF-path is 51 mW, with the 1st-LNTA and Rauch using 35% and 30% of that power, respectively. Despite all the increased configuration options, power consumption remains constant. While in the case of the HF-path, the power consumption for the minimum baseband gain drops from 68 mW to 56 mW as the baseband gain decreases. This is because the current mirror branches of the open-loop filter are turned off. The power consumption, on the other hand, is unaffected by the front-end gain variation and remains unchanged when the gain is reduced. The I-Q BB section of the HF-path uses more than 64% of the total power (Fig.4.18b).

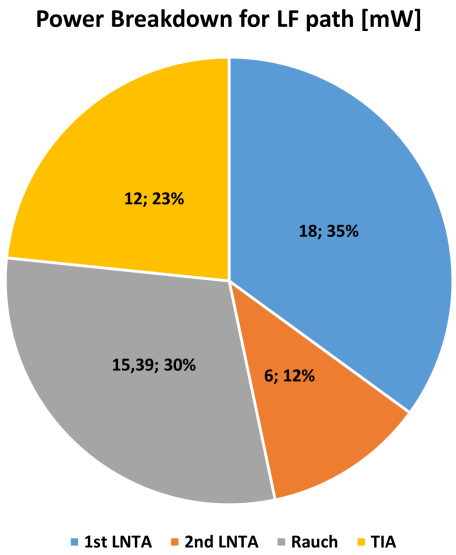

(a)

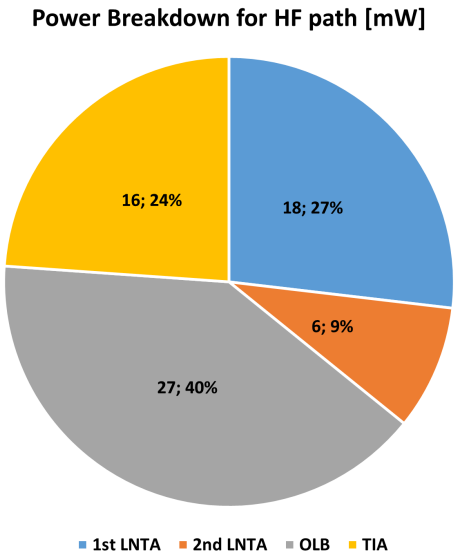

(b)

Figure 4.18: (a) Power distribution for maximum Rx gain - LF path (b) Power distribution for maximum Rx gain - HF path.

Conclusions

For the 5G wireless standard and beyond, a highly linear TIA design is presented in this thesis. The objective was to design a TIA that can satisfy the bandwidth and linearity requirements set forth by the new wireless standards. Additionally, it described the wireless receiver architecture for 5G applications; the receiver is based on RF signal direct-conversion. Covering the channel bandwidth between 50MHz and 2GHz while maintaining linearity and noise requirements within the specifications.

The presented TIA is based on OTA closed in a feedback loop. The OTA is based on FeedForward compensation approach, eliminating bandwidth constraint brought on by Miller capacitors, to increase the benefit of closed-loop operating over a broad-band. Inside the OTA, inductive peaking is employed to provide stability without increasing power consumption. The benefit of this approach is that it can provide a TIA with a bandwidth of up to 1.5GHz, IB IIP3 that is always over 35dBm, and compression that is nearly rail-to-rail with a power consumption of 17mW. The broad and configurable bandwidth of this TIA makes it appropriate for 5G and next-generation wireless communications.

The receiver is designed using a current mode direct-conversion architecture. The front-end of this architecture is based on two cascaded cross-coupled LNTAs with an 80mS RF transconductance gain to offer good noise performance. The low frequency (LF - RF chan. BW 50MHz - 400MHz) and high frequency paths (HF - RF chan. BW 800MHz - 2000GHz) baseband sections of the receiver cover channel bandwidth from 50MHz to 2GHz. The measurement results for the receiver, which was built using TSMC 28nm technology, are in perfect accordance with the design requirements. The receiver has a gain configuration range of 45dB to 0dB with OOB selectivity between band-edge and 4 times the band-edge more than 33 dB. IB-OIP3 exceeds 21dBm in all gain and bandwidth configurations. The receiver, for maximum gain and

bandwidth, have an integrated noise figure of less than 6dB, with a slope of less than 0.7dB/dB of noise increase for every dB of gain decrease. Based on these results, the receiver appears to be a strong contender for 5G wireless transceivers.

Bibliography

[1] B. Razavi, *RF Microelectronics, 2ne ed.* Prentice Hall Press Upper Saddle River, NJ, USA, 2011.

[2] C. E. Shannon, "Communication in the presence of noise," *Proceedings of the IEEE*, vol. 86, pp. 447–457, 1998.

[3] Y. F. H. R. E. Sheriff, *Mobile Satellite Communications.* Chichester, England: John Wiley & Sons, 2001.

[4] K. Santhi, V. Srivastava, G. SenthilKumaran, and A. Butare, "Goals of true broad band's wireless next wave (4g-5g)," in *2003 IEEE 58th Vehicular Technology Conference. VTC 2003-Fall (IEEE Cat. No.03CH37484)*, vol. 4, 2003, pp. 2317–2321 Vol.4.

[5] Q. T. Inc., "The Evolution of Mobile Technologies: 1G to 2G to 3G to 4G LTE," https://www.qualcomm.com/content/dam/qcomm-martech/dm-assets/documents/the_evolution_of_mobile_technologies-wireless-networks.pdf, 06 2014.

[6] *Digital cellular telecommunications system (Phase 2+); Radio transmission and reception (GSM 05.05 version 8.5.1 Release 1999).* ETSI EN 300 910, Tech. Rep.,v8.5.1, 2000.

[7] J. M. T. Halonen, J. Romero, *GSM, GPRS and EDGE Performance: Evolution towards 3G/UMTS.* Chichester, England: John Wiley & Sons, 2013.

[8] *Universal Mobile Telecommunications System (UMTS); User Equipment (UE) radio transmission and reception (TDD) (3GPP TS 25.102 version 11.3.0 Release 11).* ETSI TS 125 102, Tech. Rep., v11.3.0, 2012.

[9] H. Holma and A. Toskala, *WCDMA for UMTS: HSPA Evolution and LTE.* Chichester, England: John Wiley & Sons, 2010.

[10] J. Lee, Y. Kim, Y. Kwak, J. Zhang, A. Papasakellariou, T. Novlan, C. Sun, and Y. Li, "Lte-advanced in 3gpp rel -13/14: an evolution toward 5g," *IEEE Communications Magazine*, vol. 54, no. 3, pp. 36–42, 2016.

[11] Q. T. Inc., "What's in the future of 5G?" https://www.qualcomm.com/content/dam/qcomm-martech/dm-assets/documents/powerpoint_messaging_-_whats_in_the_future_of_5g_web.pdf, 10 2019.

[12] *5G; NR; User Equipment (UE) radio transmission and reception; Part 1: Range 1 Standalone (3GPP TS 38.101-1 version 15.3.0 Release 15).* ETSI TS 138 101-1, V15.3.0, 10 2018.

[13] *5G; NR; User Equipment (UE) conformance specification; Radio transmission and reception; Part 2: Range 2 standalone (3GPP TS 38.521-2 version 15.2.0 Release 15).* ETSI TS 138 521-2, V15.2.0, 05 2019.

[14] M. Valla, G. Montagna, R. Castello, R. Tonietto, and I. Bietti, "A 72-mw cmos 802.11a direct conversion front-end with 3.5-db nf and 200-khz 1/f noise corner," *IEEE Journal of Solid-State Circuits*, vol. 40, no. 4, pp. 970–977, 2005.

[15] H. Khatri, P. S. Gudem, and L. E. Larson, "Distortion in current commutating passive cmos downconversion mixers," *IEEE Transactions on Microwave Theory and Techniques*, vol. 57, no. 11, pp. 2671–2681, 2009.

[16] I. Fabiano, M. Sosio, A. Liscidini, and R. Castello, "Saw-less analog front-end receivers for tdd and fdd," *IEEE Journal of Solid-State Circuits*, vol. 48, no. 12, pp. 3067–3079, 2013.

[17] D. Murphy, H. Darabi, A. Abidi, A. A. Hafez, A. Mirzaei, M. Mikhemar, and M.-C. F. Chang, "A blocker-tolerant, noise-cancelling receiver suitable for wideband wireless applications," *IEEE Journal of Solid-State Circuits*, vol. 47, no. 12, pp. 2943–2963, 2012.

[18] N. N. Miral, D. Manstretta, and R. Castello, "A 17 mw 33 dbm ib-oip3 0.5-1.5 ghz bandwidth tia based on an inductor-stabilized ota," in *ESSCIRC 2021 - IEEE 47th European Solid State Circuits Conference (ESSCIRC)*, 2021, pp. 203–206.

[19] ——, "A 17-mw 0.5–1.5-ghz bandwidth tia based on an inductor-stabilized ota with 35–42-dbm in-band iip3," *IEEE Solid-State Circuits Letters*, vol. 5, pp. 13–16, 2022.

[20] R. G. H. Eschauzier and J. H. Huijsing, "Frequency compensation techniques for low-power operational amplifiers," 1995.

[21] Y. Dong, J. Zhao, W. W. Yang, T. Caldwell, H. Shibata, Z. Li, R. Schreier, Q. Meng, J. B. Silva, D. Paterson, and J. C. Gealow, "A 72 db-dr 465 mhz-bw continuous-time 1-2 mash adc in 28 nm cmos," *IEEE Journal of Solid-State Circuits*, vol. 51, no. 12, pp. 2917–2927, 2016.

[22] G. Pini, D. Manstretta, and R. Castello, "Analysis and design of a 20-mhz bandwidth, 50.5-dbm oob-iip3, and 5.4-mw tia for saw-less receivers," *IEEE Journal of Solid-State Circuits*, vol. 53, no. 5, pp. 1468–1480, 2018.

[23] J. Harrison and N. Weste, "A 500 mhz cmos anti-alias filter using feedforward op-amps with local common-mode feedback," in *2003 IEEE International Solid-State Circuits Conference, 2003. Digest of Technical Papers. ISSCC.*, 2003, pp. 132–483 vol.1.

[24] J. Lechevallier, R. Struiksma, H. Sherry, A. Cathelin, E. Klumperink, and B. Nauta, "5.5 a forward-body-bias tuned 450mhz gm-c 3rd-order low-pass filter in 28nm utbb fd-soi with ¿1dbvp iip3 over a 0.7-to-1v supply," in *2015 IEEE International Solid-State Circuits Conference - (ISSCC) Digest of Technical Papers*, 2015, pp. 1–3.

[25] T.-Y. Lo and C.-C. Hung, "A 1 ghz ota-based low-pass filter with a high-speed automatic tuning scheme," in *2007 IEEE Asian Solid-State Circuits Conference*, 2007, pp. 408–411.

[26] H. Jung, D. R. Utomo, S.-K. Han, J. Kim, and S.-G. Lee, "An 80 mhz bandwidth and 26.8 dbm oob iip3 transimpedance amplifier with improved nested feedforward compensation and multi-order filtering," *IEEE Transactions on Circuits and Systems I: Regular Papers*, vol. 67, no. 10, pp. 3410–3421, 2020.

[27] K. Sohal, "Design of wideband cmos direct-conversion receiver for 5g wireless applications," 2021.

[28] I. Fabiano, M. Sosio, A. Liscidini, and R. Castello, "Saw-less analog front-end receivers for tdd and fdd," *IEEE Journal of Solid-State Circuits*, vol. 48, no. 12, pp. 3067–3079, 2013.

[29] K. Sohal, D. Manstretta, and R. Castello, "A 2nd order current-mode filter with 14db variable gain and 650mhz to 1ghz tuning-range in 28nm cmos," in *2021 IEEE International Symposium on Circuits and Systems (ISCAS)*, 2021, pp. 1–5.

[30] M. D. Salehi, "Design of highly linear and low power base-band filters for high bandwidth current-mode receivers," 2020.